Charge Separation and Singlet Fission in Covalently Linked Diketopyrrolopyrrole Derivatives and Triphenylamine Triad in Solution

Madhu Chakali, Haraprasad Mandal, Munisamy Venkatesan,
Bharath Dyaga, V. Jayathirtha Rao, Prakriti Ranjan Bangal

PII: S1010-6030(20)30814-5
DOI: https://doi.org/10.1016/j.jphotochem.2020.113017
Reference: JPC 113017

To appear in: *Journal of Photochemistry & Photobiology, A: Chemistry*

Received Date: 3 July 2020
Revised Date: 26 October 2020
Accepted Date: 29 October 2020

Please cite this article as: Chakali M, Mandal H, Venkatesan M, Dyaga B, Rao VJ, Bangal PR, Charge Separation and Singlet Fission in Covalently Linked Diketopyrrolopyrrole Derivatives and Triphenylamine Triad in Solution, *Journal of Photochemistry and amp; Photobiology, A: Chemistry* (2020), doi: https://doi.org/10.1016/j.jphotochem.2020.113017

Charge Separation and Singlet Fission in Covalently Linked Diketopyrrolopyrrole Derivatives and Triphenylamine Triad in Solution

Madhu Chakali [a,b], Haraprasad Mandal[a,b], Munisamy Venkatesan [a,b], Bharath Dyaga[§], V. Jayathirtha Rao[*§], Prakriti Ranjan Bangal[a,b*]

[a] Department of Analytical and Structural Chemistry, CSIR-Indian Institute of Chemical Technology, Uppal Road, Tarnaka, Hyderabad. 500007, India.

Email: prakriti@iict.res.in

[b] Academy of Scientific and Innovative Research (AcSIR), Ghaziabad - 201002, India.

[§] Fluoro-Agrochemical Division, CSIR-Indian Institute of Chemical Technology, Uppal Road. Email: vaidya.opv@gmail.com

Graphical Abstract

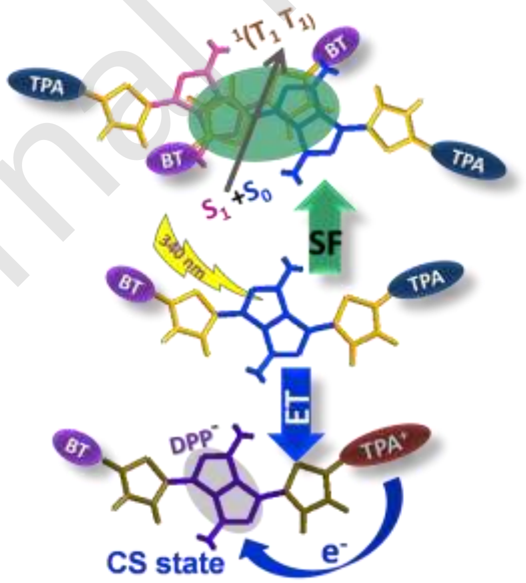

Highlight

- We have designed and synthesized a diketopyrrolopyrrole (DPP) based asymmetric push-pull triad system (BT-DPP-TPA(7)) comprising diketopyrrolopyrrole, triphenylamine, benzothiophene and thiophene.

- Ultrafast relaxation dynamics of the central DPP derivative, TDPP(4) and BT-DPP-TPA(7) triad system have been explored in solution phase by femtosecond transient absorption spectroscopy.

- Upon photoexcitation to DPP moiety of BT-DPP-TPA(7) photoinduced reductive electron transfer occurs from ground state TPA to excited singlet state of DPP leading to long-lived CS state.

- Apart from this event, we demonstrate for the first time that TDPP(4) as well as BT-DPP-TPA(7) take part in SF in the solution phase in 100-200 ps time scale in the solution of the concentration on and above 100 µM.

- These combined rare features in BT-DPP-TPA(7) may have implications for improving the efficiency of photovoltaic devices using DPP derivatives.

Abstract

A covalently linked push-pull type triad containing two unsymmetrical electron donors, triphenylamine (TPA) and benzothiophene (BT), and diketopyrrolopyrrole (DPP), an electron acceptor, through thiophene spacer has been synthesized (BT-DPP-TPA(7)) and ultrafast relaxation dynamics of the triad has been explored in solution phase by various spectroscopic methods. Steady-state and time-resolved emission studies show the efficient fluorescence quenching of the DPP entity of as prepared BT-DPP-TPA(7) triad. The negative free energy values comprising the redox potentials and singlet state energy of BT-DPP-TPA(7) revealed the probability of electron transfer from the singlet ground state of TPA to the excited singlet state of DPP. Femtosecond transient absorption (*fs*TA) spectroscopic studies confirmed the formation of charge separation state by detecting triphenylamine radical cation as electron-transfer transients. The rate of charge separation, k_{CS}, is (10^9−10^8 s^{-1}) observed to be increasing from nonpolar to polar solvents and the rate of charge recombination, k_{CR}, was found to be slower (μs time scale) in polar solvents like DMF and chloroform, than that in hexane, non-polar solvent (ns time scale). This novel aspect could be due to asymmetrically designed push-pull type triad, a feature that was not evident in push-pull triad constructed using symmetric TPA as electron donors. Furthermore, *fs*TA studies also demonstrate, for the first time, that the DPP derivatives, TDPP(4) and BT-DPP-TPA(7), both undergo singlet fission (SF) event (S→TT) in 100-200 ps time scale in solution phase for the solution of concentration above ~100 μM. These results may pave the new avenue for device design comprising DPP derivatives.

Keywords: Diketopyrrolopyrrole (DPP), Charge Sseperation, Singlet Fission, Concentration, Transient absorption

1. Introduction

In the last few decades, 3,6-diaryl-2,5-dihydro-1,4-diketopyrrolo[3,4-c] pyrrole (DPP) derivatives have emerged as one of the important pigment in many different fields of applications, such as inks, paints, plastic [1-4], and laser dyes [5-6], due to their excellent thermal as well as photo-stabilities and glaring photophysical properties. However, currently, DPP derivatives are attracting considerable research efforts in the field of organic electronic materials due to its ambipolar nature and electron accepting as well as electron donating abilities along with the aforementioned properties. In view of replacing semiconductor solar cells, metal-free dye-sensitized solar cell [7-17] (DSSC) has emerged as a promising alternative source to fulfill the ever increasing demand for green and clean energy for a sustainable civilization. In the quest to have good sensitizer for DSSC in terms of high solar energy conversion efficiency and low cost of production, the design and development of a large array of π-conjugated organic materials with DPP as core unit and testing of their device performances have rejuvenated the importance of DPP molecules in DSSC research community [18-20]. Very recent DPP derivatives are accredited as singlet fission (SF) chromospheres,[21-23] where a singlet excited state energetically down-converts in spin-allowed process yielding two triplet excitons on adjacent molecules (Scheme 1) of proper orientation when energy of the singlet state is greater than or equal to two times that of the triplet state, $E(S_1)\geq 2E(T_1)$. Till date, triplet quantum yield up to 200% has been achieved in single crystal, solid film, nano-aggregate, assembly of two or more chromophores in solution by SF [24]. As a result, it is predicted that SF can lead a probable way to cross-over 32% Shockley-Queisser limit of the overall efficiency of solar photovoltaics [25-27]. Interestingly, DPP derivatives are also recognized as triplet fusion chromospheres or triplet-triplet annihilator, a complimentary system of SF, where two or more low-energy triplet states are up-converted to one high energy singlet state [28]. Likewise the SF, the TF process is energetically allowed spin-conserved process so long as it satisfies $E(S_1)\geq 2E(T_1)$. However, TF eventually needs triplet sensitization by suitable sensitizer via the triplet-triplet energy transfer process. Depending upon the requirement and device design, both SF and TF are extensively exploited to the photovoltaic applications,[18-20, 29-31] among other areas of applications [32-37]. Even though the quest for new SF chromospheres has arisen as a focused research field, detailed understanding of SF mechanism, electronic couplings between adjacent SF chromospheres with proper geometric orientations, and intermediate excited states involved in the process are still lacking.

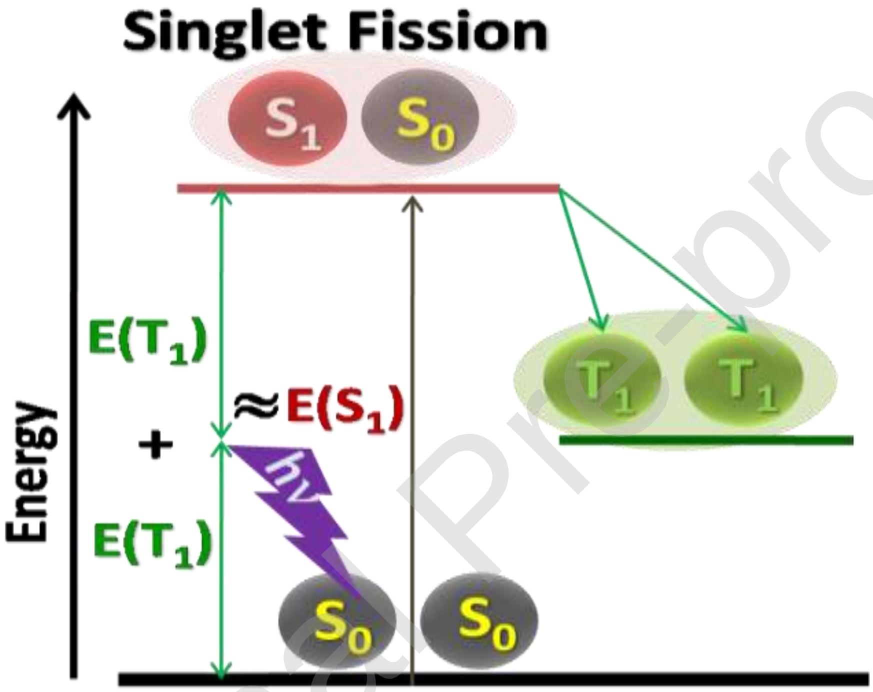

Scheme 1. Schematic energy diagram of singlet fission.

For a donor-acceptor (D-A) based efficient organic photovoltaic devices free charge generation is created upon photoexcitation yielding very fast charge-separated (CS) states and excitation decay to the triplet state is considered as an unwanted energy loss process. On the contrary, a direct photoexcitation to triplet state or triplet sensitization is advantageous for multiexciton harvesting in singlet fission photovoltaics and the formation of CS state is considered as an obstructing factor for multiple triplet generation. When these two extreme events are present in a D-A based system then it is expected that such a system can provide important insights into the mechanism of free charge generation and charge recombination (CR) in OPVs. Fortunately, D-A based system containing the DPP as core unit is highly potent to those extreme events and yields fast CS state and slow CR along with the efficient spin-conversion process, SF and TF [20]. In spite of immense literature available on DPP where it has been considered as an important organic building block to construct high performance materials for photovoltaic applications,[20-31] the photophysical relaxation dynamics and the dynamics of charge separation and charge recombination in DPP based systems are relatively spare [38-41]. In this connection, we have designed and synthesized a covalently linked push-pull type triad containing two unsymmetrical donors, triphenylamine (TPA) and benzothiophene (BT), and diketopyrrolopyrrole (DPP) as an acceptor with thiophene as a spacer and explore the CS, CR and SF dynamics of as prepared triad employing steady state and femtosecond transient absorption spectroscopic measurements. Global and target analysis of TA data provides the Spectro temporal information which can reveal the structure−property relationship of widely used moieties in the design of efficient optoelectronic materials. This study may be relevant to a wide range of fundamental research and applications pertaining to DPP derivatives.

2. Experimental Section

2.1. Materials and instruments

All the solvents and analytical grade reagents were obtained from commercial sources, Sigma-Aldrich (USA), and used without further purification. UV−Vis absorption and fluorescence emission spectra were recorded at room temperature on a Hitachi U-2910 (Japan) spectrophotometer and a Fluorolog-3 spectrofluorimeter of Horiba Jobin Yvon

(France), respectively. The absorption and fluorescence measurements were carried out in different solvents with increasing solvent polarity from hexane to methanol. To ascertain the reproducibility of data, absorption and emission experiments were repeated in three different days with freshly prepared samples and every time data are found to be identical.

2.2. Cyclic Voltammetry

The electrochemical experiments were performed using a PC-controlled CHI 620C electrochemical analyzer (CH instruments) in 1 mM solution of degassed dry dichloromethane at a scan rate of 100 mV s^{-1} using 0.1 M, Tetrabutylammonium perchlorate (TBAP) as the supporting electrolyte. The glassy carbon, Ag/AgCl, and platinum wire were used as the working electrode, reference electrode, and counter electrode respectively.

2.3. Time-resolved Fluorescence Measurements

The fluorescence lifetime measurements were carried out using TCSPC method in nanosecond time scale. The ~100 fs pulses with an 8 MHz repetition rate are obtained Ti:sapphire oscillator (Spectra Physics, MaiTai, 100fs, 80MHz) output using the femtosecond Pulse Selector (3980-5S, Spectra Physics). The sample was excited at 390 nm, which were generated by frequency doubling of 780 nm Ti: sapphire output with a 0.5 mm BBO crystal. The time distribution of fluorescence intensity data was recorded on an SPC-130 TCSPC module (Becker and Hickl). The IRF (Instrument Response Function) value of this time correlated single photon counting was about 200 ps.

2.4. Transient Absorption/Pump−Probe

Transient absorption studies were performed using a pump−probe set up (ExciPro) of CDP Systems Corporation (Moscow) and described elsewhere [42]. In brief, the output of the optical parametric amplifier (TOPAS prime) was used as a pump source at the required wavelength and fed into the spectrometer through a synchronized chopper at 1kHz repetition rate. A lens (f = 200 mm) was used to adjust the pump diameter, while an iris and neutral density filter combination were used to adjust the pump energy. A Berek's variable wave plate was placed in the pump beam, and polarization was fixed at magic angle with respect to probe pulse. A part of the output of Ti:sapphire (f = 150 mm) was used to focus both probe and reference beams to the rotating sample cell. Two lenses (f = 60 mm) made probe and reference images at the entrance surfaces of two optical fibers, which are connected to the entrance slit of the imaging spectrometer (CDP-2022i). This spectrometer consists of UV−vis photodiode (Si linear photodiode) arrays and IR photodiode (GaAs linear photodiode) array with Spectral response range 200−1000 and 900−1700 nm, respectively. Quartz cells of 1 mm sample path length were used for all studies, and IRF was estimated to be ≤150 fs. However, to minimize the solvent signal, pump pulse energy was kept below 3μJ/s and probe pulse energy was from 0.1 to 0.5 μJ at the sample. For transient absorption spectra, the group velocity dispersion compensation of the white light continuum (probe beam) was done using the studied solvent's two photon absorption data for a few picoseconds delay.

2.5. Global and Target Analysis of Transient Data

In order to estimate precise rate constants and species-related spectral signatures, the transient data reported in this paper were analyzed using a combination of global and target analysis [43,44]. With the aim of predicting the minimum number of components involved in the evolution of the transient data, firstly, global analysis was performed via two different approaches based on the principle of superposition of the least number of independent exponential components, which provided a straightforward description of the data at all measured wavelengths and all time points simultaneously. The number of independent components fitted to all the data was determined by gradually increasing the number of exponential components until the residuals were effectively zero. The simplest description in global analysis used a parallel kinetic model, in which a number of monoexponentially decaying independent components, each of which was represented by a single rate constant (reciprocal of the lifetime) and amplitude at each recorded wavelength, yielded decay-associated difference spectra. The decay-associated difference spectra represented the growth and decay of the components with their corresponding decay constants and lifetime values. A second sequential kinetic model, namely, an unbranched unidirectional model, consisted of successive monoexponential decays with increasing time constants and estimated the gross spectral evolution of the data to generate evolution associated difference spectra. Finally, the data were fitted to a full kinetic model (compartmental scheme) in target analysis by a combination of the parallel and sequential kinetic models of global analysis, which included all possible branching routes and equilibria between compartments to specify the microscopic rate constants that described the decay of the compartments, as well as the transfer of excitation between the compartments. This analysis estimated the real spectra of each compartment (excited species), which are termed species-associated difference spectra (SADS). In target analysis of ET systems, equality between the total rates of CS and CR is constrained to fit the proposed scheme andindividual rates are free to be optimized to generate the spectra and lifetimes of the respective states. The entire global and target analysis was performed with the R package TIMP and its graphicaluser interface Glotaran (for details, see the literature [45–47].

2.6. Synthesis

The synthesis of 3-(5-(benzo[b]thiophen-2-yl) thiophen-2-yl)-6-(5-(4-(diphenylamino) phenyl) thiophen-2-yl)-2,5-bis(2-ethylhexyl)pyrrolo[3,4-c]pyrrole-1,4(2H,5H)-dione (BT-DPP-TPA (7) is done following the synthetic route as shown in Scheme-2. First we have synthesizes 4-(4,4,5,5- tetramethyl-1,3,2- dioxaborolan-2-yl)triphenylamine (1), 2-(benzo[b]thiophen-2-yl)-4,4,5,5-tetramethyl-1,3,2-dioxaborolane (2), 3,6-Di(thiophen-2-yl)pyrrolo[3,4-c]pyrrole-1,4(2H,5H)-dione (3), 2,5-Bis(2-ethylhexyl)-3,6-di(thiophen-2-yl)pyrrolo[3,4c]pyrrole-1,4(2H,5H)-dione(TDPP-2) (4), 3,6-bis(5-bromothien-2-yl)-2,5-bis(2-ethylhexyl)pyrrolo[3,4-c]pyrrole-1,4(2H,5H)-dione (5) according to the literature method describe elsewhere [48].

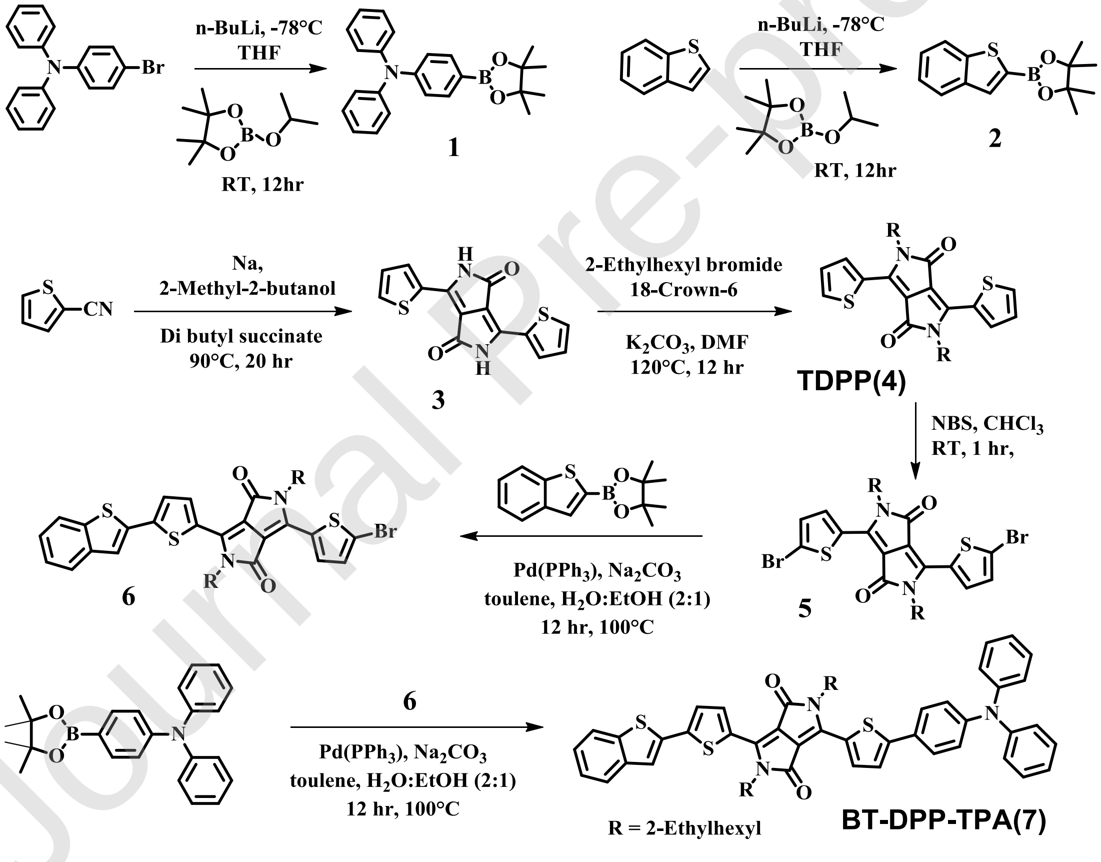

Scheme 2. Schematic diagram of synthetic route to prepare BT-DPP-TPA (7)

3-(5-(benzo[b]thiophen-2-yl)thiophen-2-yl)-6-(5-bromothiophen-2-yl)-2,5-bis(2-ethylhexyl)pyrrolo[3,4-c]pyrrole-1,4(2H,5H)-dione (6). The compound (6) was synthesized following Suzuki coupling reaction. In a 250 ml round bottom flask, the mixture of 3,6-bis(5-bromothiophen-2-yl)-2,5-bis(2-ethylhexyl) pyrrolo[3,4-c] pyrrole-1,4(2H,5H)-dione (5), (2g, 2.93 mmol) and 2-(benzo[b]thiophen-2-yl)-4,4,5,5-tetramethyl-1,3,2-dioxaborolane (0.76g, 2.93 mmol), $Pd(PPh_3)4$ (67 mg), Na_2CO_3 (4.95 g, 460 mmol) in toluene (70 ml), was degassed with N_2 for 30 min. Then H_2O + EtOH (44.5mL 2:1 ratio degassed for 30 min.) added to the reaction mixture. The reaction mixture was again degassed with N_2 for 30 min and heated to 90 °C for 14 hours. Reaction was monitored using TLC, after completion of reaction, the solution was washed with $CHCl_3$ and H_2O, the organic extract with $CHCl_3$, dried over Na_2SO_4, the solvent was removed under reduced pressure. The residue was purified by column chromatography using hexane: EtOAc (98: 2) as the eluent. ^{1}H NMR (300 MHz, $CDCl_3$): δ 8.95 (s, 1H), 8.65 (s, 1H), 7.90-7.71 (m, 2H), 7.56 (s, 1H), 7.48-7.32 (m, 3H), 7.23 (s, 1H), 4.12-3.93 (m, 4H), 1.99-1.83 (m, 2H), 1.46-1.25 (m 18H), 0.99-0.84 (m, 12H) (Fig. S14).

3-(5-(benzo[b]thiophen-2-yl)thiophen-2-yl)-6-(5-(4-(diphenylamino) phenyl) thiophen-2-yl)-2,5-bis(2-ethylhexyl) pyrrolo[3,4-c]pyrrole-1,4(2H,5H)-dione, {BT-DPP-TPA (7)}: The final compound BT-DPP-TPA (7) was again prepare from (6) using Suzuki coupling reaction as described. 3-(5-(benzo[b]thiophen-2-yl)thiophen-2-yl)-6-(5-bromothiophen-2-yl)-2,5-bis(2-ethylhexyl) pyrrolo[3,4-c]pyrrole-1,4(2H,5H)-dione, (6), (0.27 mmol) and equivalent borolane derivative (0.32 mmol) and $Pd(PPh_3)4$ (5mol %) were dissolved in toluene (20 mL). The mixture was purged with N_2 gas for 15 min. To this 2M K_2CO_3 was added and purged with N_2 gas for 30 min and refluxed (120 °C) for 14 hours.

Reaction was monitored using TLC, after completion of reaction, the reaction mixture was washed with $CHCl_3$ and H_2O, the organic extract with $CHCl_3$, dried over Na_2SO_4, and the solvent was removed under rotary vacuum. The residue was washed with MeOH several times and recrystallization in toluene. 1H NMR (300 MHz, $CDCl_3$): δ 9.04 (d, J = 4.27 Hz, 1H), 8.90 (d, J = 4.12 Hz, 1H), 7.83-7.80 (m, 1H), 7.79-7.76 (m, 1H), 7.55-7.53 (m, 2H), 7.53 (s, 1H), 7.44-7.42 (d, J = 4.27 Hz, (Fig. S15).

MALDI-MS (positive mode, m/z): found (M^+H^+) 900.69, calc. for $C_{56}H_{57}N_3O_2S_3$, is 899.3613. (Fig. S16).

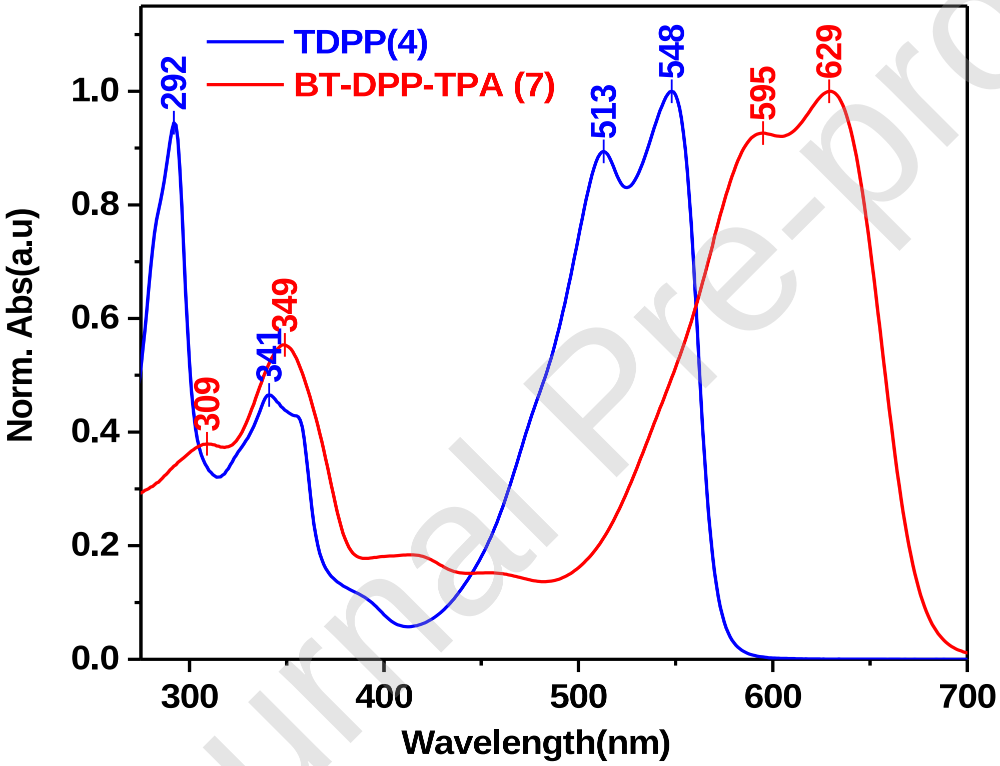

Fig. 1. Normalized Uv-Vis absorption spectra of TDPP (4) and BT-DPP-TPA (7) in Chloroform.

3.RESULTS

3.1 Steady-State Absorption and Emission

The ground state absorption spectra of reference compound thiophene substituted TDPP (4) and donor-acceptor-donor (D-A-D) type triad BT-DPP-TPA (7) are recorded in different solvents with varying polarities (Fig. S1) and the peak positions are summarized in Table 1. Fig. 1 shows typical normalized ground state absorption spectra of TDPP (4) and BT-DPP-TPA (7) triad in chloroform solution (10μM) respectively. As shown in Fig. 1, the characteristic absorption spectra of TDPP (4) consist of three distinct bands: a strong high energy band at ~290 nm (S_3), which arises due to n→π* transitions and the relatively weak second absorption maxima appears in the range of 310 to 405 nm region with two vibrational peaks at 341, 357 nm and one shoulder peak at ~383 nm which is assigned to S_2 state and it is attributed to π→π* transition of core DPP [49] moiety. Finally, the third broad and intense low energy band emerges around 450-600 nm region which shows two distinct peaks at ~513 and ~547 nm. The origin of this characteristic long wavelength absorption band of DPP derivatives is consistent with the π→π* transitions and it is due to intramolecular charge transfer (ICT) from thiophene moiety to DPP lactam unit [49,50]. This low energy band is attributed to S_1 (ICT) state. Ongoing from nonpolar to polar solvent a slight blue shift for all the absorption peaks of TDPP(4) is observed along with the reduction of structure of the spectra corresponds to low energy band. The absorption spectra of BT-DPP-TPA(7) triad show a similar type of band patterning as observed in TDPP(4). Relatively weak higher energy bands (S_3 and S_2) of BT-DPP-TPA(7) are found to be peaking at ~309 and 350 nm respectively and intense low energy broad band is observed to be in between 500-600 nm region with large bathochromic shift (~80 nm) with respect to that of TDPP(4) (Fig. 1). The peak position of two characteristic vibronic structures are recorded to be at 592 and 630 nm respectively. The vibrational fine structures for both high energy and low energy bands are reduced significantly in BT-DPP-TPA(7) triad with respect to TDPP(4) in all the solvents studied. These vibrational fine structures reduce further on increasing the solvent polarity along with 3-4 nm of blue shift of all absorption peaks. These results can be associated with the charge transfer behavior between TPA/BT donors and DPP acceptors, thus resulting in delocalization of charge in the ground state over the backbone between donor and acceptor moieties. Furthermore, in higher energy side i.e. below 325 nm region, a modulation of absorption spectra is observed which is due to the overlapping of TPA/BT absorption to DPP absorption and this modulation of absorption spectra again confirms the undergoing electronic interaction between TPA/BT and DPP moieties. Note, concentration dependent absorption studies reveal that neither TDPP (4) nor BT-DPP-TPA(7) shows any noticeable change in the shape of absorption spectra on increasing concentration up to 50-70 µM. However, upon increasing further concentration (from 100 µM to 1 mM) a slight change in the shape of absorption spectra of both the compounds is observed. The intensity ratio of two prominent vibronic peaks at lower energy absorption band of respective molecules starts changing along with increase in full width at half maxima(FWHM) of the absorption band. Although, due to very high molar absorption coefficient, absorption spectra get saturated below 1 mM concentration when studied in 10 mm cuvette(for detail see Fig S2 and Fig.S3.). However, these results can be combined to the fact that in higher concentration, approximately above 60-70 µM of concentration, both the molecules could start forming aggregation in the ground state.

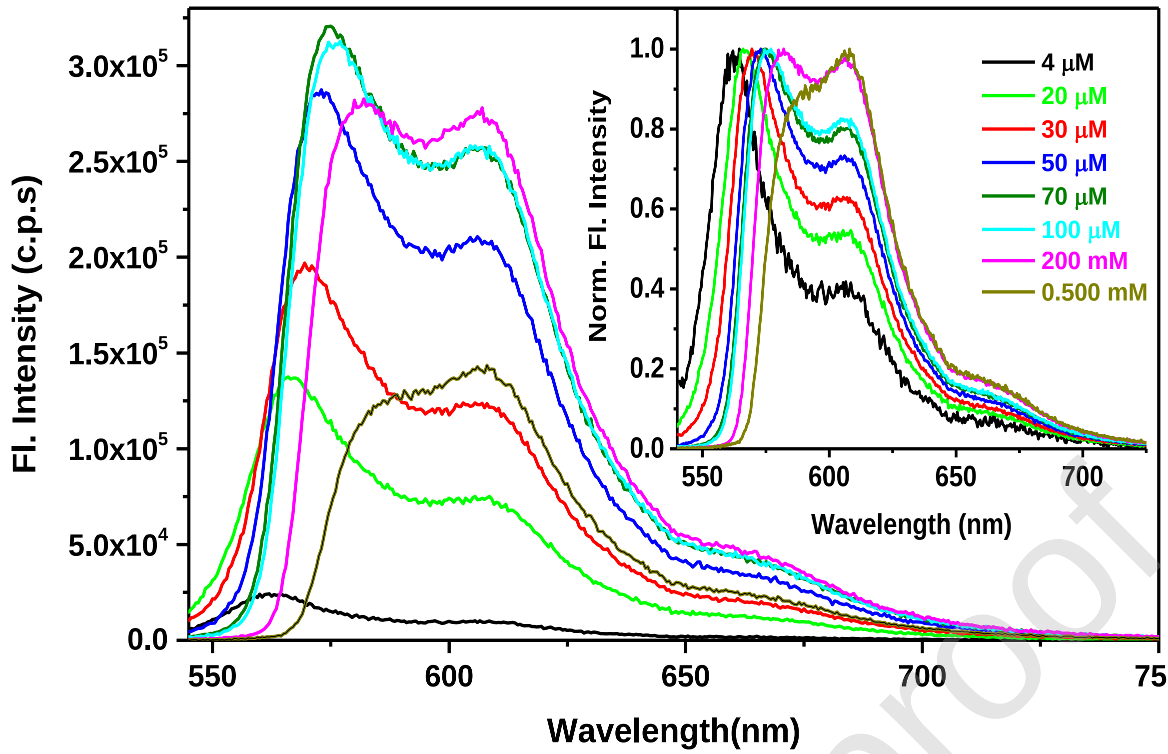

Fig.2. Concentration dependent fluorescence emission spectra of TDPP(4) in Chloroform solution λ_{EX}= 450 nm. Inset shows normalized fluorescence emission spectra as a function of concentration.

The dilute solutions (~10^{-5}µM) of TDPP(4) exhibits very strong fluorescence emission in different solvents with a characteristics peak at around 550 nm region and a shoulder band at around 600 nm (Fig. S4) when excited at any wavelength of the absorption band. All these fluorescence emission peaks show a systematic redshift on increasing solvent polarities and they are summarizing in table 1. The fluorescence quantum yield (φ_{fl}) of TDPP(4) is estimated to be ~70% in the non-polar solvents and it slightly reduces in polar solvents confirming intramolecular interaction between thiophene and DPP moiety [51,52]. Fig. 2 shows the concentration dependent fluorescence spectra TDPP(4) in chloroform solution when excitation wavelength is selected to a low absorption reagion of 450 nm to reduce the inner filter effect for concentrated. As shown in Fig.2, the intensity of fluorescence emission increases initially on increasing concentration but after 60-70 µM of concentration TDPP (4) the fluorescence intensity starts decreasing. More significantly, the higher energy fluorescence emission peak of TDPP (4) shows gradual redshift on increasing concentration and it becomes more prominent after 60-70 µM concentration. These redshift of emission peak and prominent decrease of fluorescence intensity after 60-70 µM can be attributed to the effect of the formation of aggregation in higher concentration. It is important to note that the rate of the intrinsic intersystem crossing of TDPP is very slow and triplet state yield is much less than 1% [53,54].

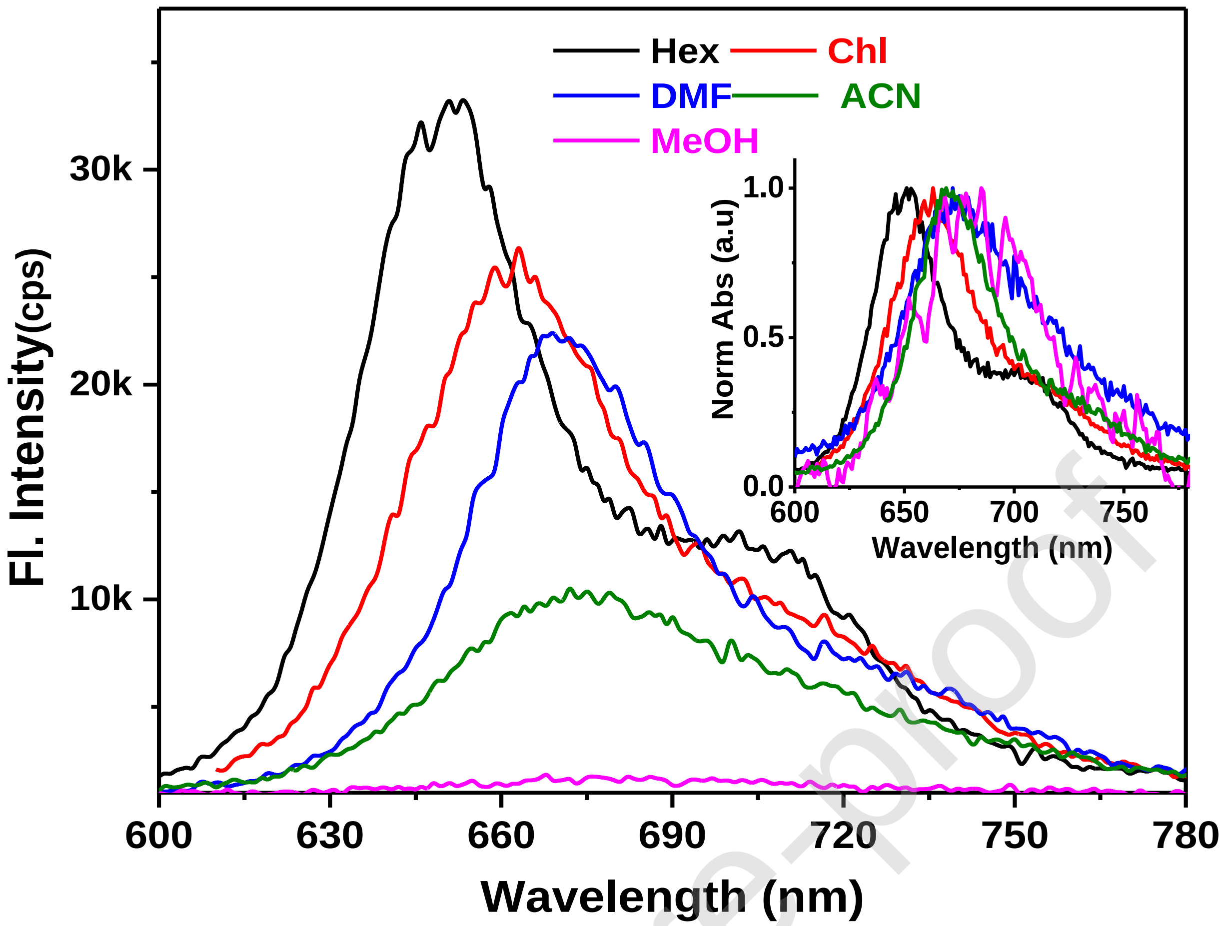

Fig. 3. Steady state fluorescence emission spectra of BT-DPP-TPA (7) (~10^{-5}M) in different solvents. Inset shows normalized emission spectra; λ_{EX}=580 nm.

The fluorescence emission spectra of equimolar solutions (~10^{-5} M) of BT-DPP-TPA(7) are recorded in different solvents of increasing polarity (Fig. 3) upon 580 nm excitation and the observed fluorescence emission peak positions and fluorescence quantum yields are listed in table 1. Likewise ground state absorption spectra, the fluorescence emission maxima of BT-DPP-TPA(7) show over 100 nm redshift with respect to that of TDPP(4). The fluorescence emission maxima of BT-DPP-TPA(7) show further bathochromic shift on going from nonpolar to polar solvents and the structured emission spectra consisting of two peaks reduce to single band emission spectra in the polar solvent. More importantly, the fluorescence emission of BT-DPP-TPA(7) is quenched enormously and the magnitude of quenching again enhanced in polar solvents (Table 1). Note, the fluorescence quenching of BT-DPP-TPA(7) in methanol, a protic solvent, is found to be very high with respect to its polarity. The fluorescence quantum yield of BT-DPP-TPA(7) in ACN is calculated to be 0.03 (φ_{fl}) whereas in methanol, relatively less polar solvent than ACN, it is observed to be 0.006(φ_{fl}). This discrepancy in solvent polarity dependent fluorescence quantum yield ongoing from aprotic solvent to protic solvent can be rationalized by probable intermolecular hydrogen bonding between methanol and triad system. However, as shown in Fig. 3, in hexane, a nonpolar solvent, BT-DPP-TPA(7) exhibits two well-resolved fluorescence emission peaks at 650 and 700 nm respectively which are consistent with emission profile of DPP derivatives although fluorescence yield quenched extensively. In polar solvents, along with large fluorescence quenching the fluorescence emission profile of BT-DPP-TPA(7) loses its fine structures which indicates the non-planer structure of BT-DPP-TPA(7) in its excited states. The electron donor units, TPA/BT, play a vital role in distorting the molecular backbone from planarity and it can be due to charge separation upon excitation to DPP unit. Hence, this quenching of fluorescence in BT-DPP-TPA(7) is attributed to photoinduced electron transfer from TPA/BT to excited DPP moiety. Furthermore, an energy transfer from the excited DPP moiety to BT or TPA is ruled out owing no overlap between the emission spectra of DPP and the absorption spectra of neither BT nor TPA.

Likewise TDPP(4), we measure fluorescence emission as a function of BT-DPP-TPA(7) concentration and observe similar kinds of results. As shown in Fig.4, the fluorescence emission intensity clearly increases on increasing BT-DPP-TPA(7) concentration up to 70 µM, and thereafter it decreases sharply on increasing concentration. Furthermore, the fluorescence emission peak shows prominent redshift after 70 µM of concentration. These results confirm that likewise TDPP (4), BT-TDPP-TPA(7) forms aggregation presumably above 70 µM of concentration.

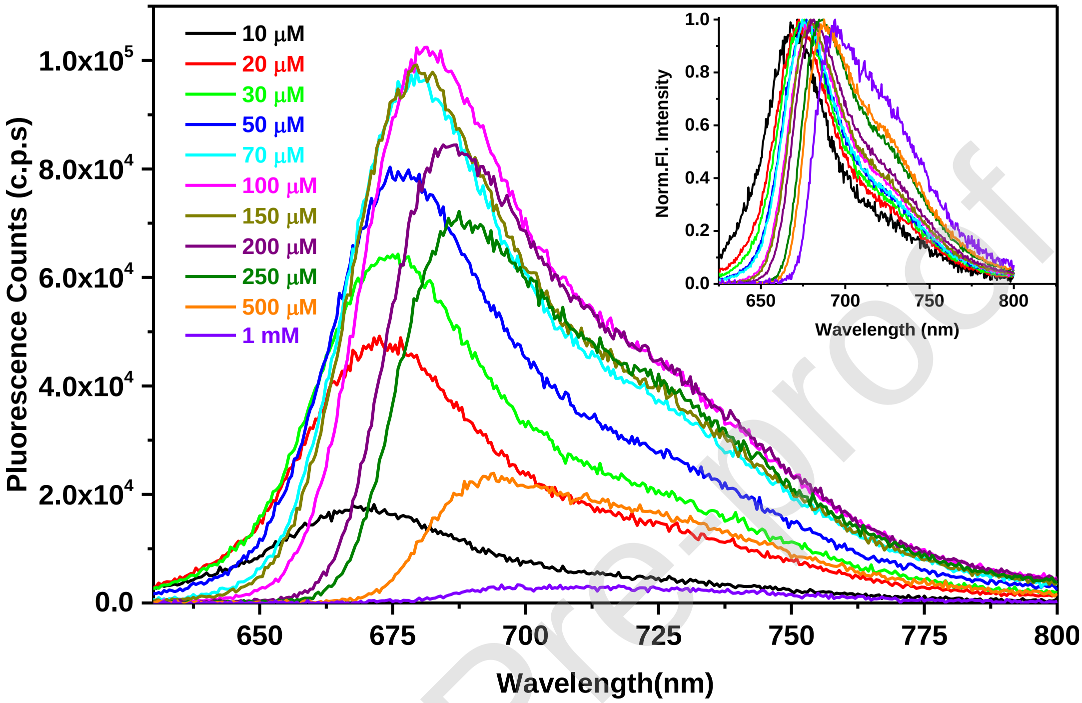

Fig.4. Concentration dependent fluorescence emission spectra of BT-DPP-TPA(7) in Chloroform solution, λ_{EX}= 530 nm. Inset shows normalized fluorescence emission spectra as a function of concentration.

The singlet state lifetimes of DPP moiety in dilute solution (10^{-5} M) TDPP(4) and BT-DPP-TPA(7) were measured in different solvents (Fig. 5) using time correlated single photon counting system(TCSPC) and they are listed in Table 1. The lowest singlet state (S_1(ICT) state) lifetime of TDPP(4) is found to be ~6.5 ns and it is almost independent of the solvent polarity. However, as shown in Fig. 5, the S_1 (ICT) state lifetime of DPP moiety in BT-DPP-TPA(7) is quenched significantly and the extent of quenching of lifetime increases further on going from nonpolar to polar solvents. These results again suggest that fluorescence quenching of BT-DPP-TPA(7) is a dynamic process which occurs in the excited state of BT-DPP-TPA(7) and it can be associated with the photoinduced electron transfer from ground state TPA/BT to excited state DPP moiety. Assuming the quenching of the fluorescence decay is due to electron transfer, the rate constant for charge separation is determined according to eq 1, and solvent dependent rate constants (k_{CS}) are listed in Table 2.

$$k_{CS} = (1/\tau_f)_{triad} - (1/\tau_f)_{ref} \quad (1)$$

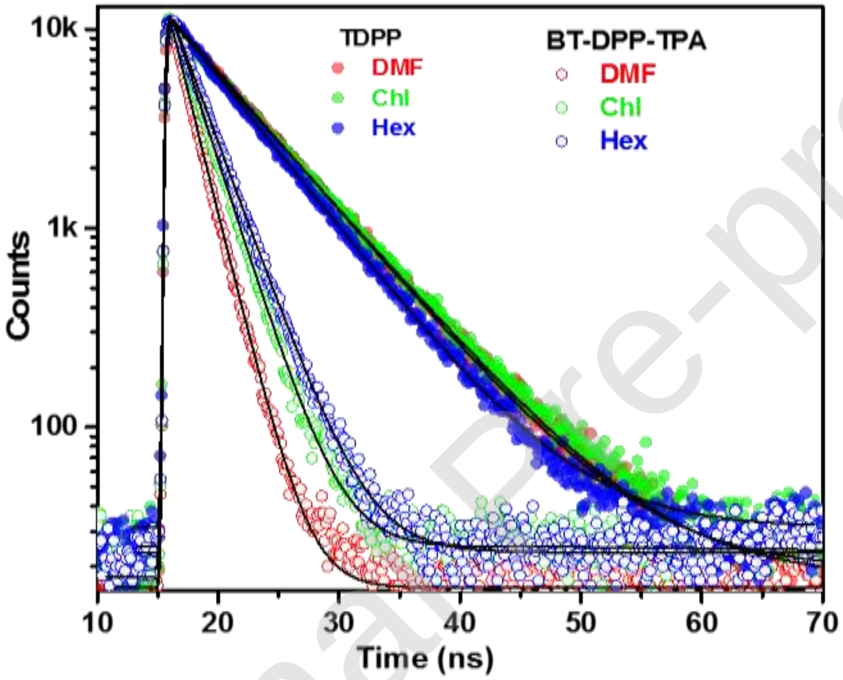

Fig. 5. Fluorescence emission decay of TDPP(4) and BT-DPP-TPA(7) in different solvents (concentration~10μM); λ_{EX}=400 nm and λ_{EM}=565 nm and 665 nm for TDPP(4) and BT-DPP-TPA (7) respectively.

In accordance with the steady-state fluorescence quenching, the quantum yield of charge separated state, Φ_{CS}, is calculated following eq 2 and it was found to be >59% in any of the studied solvents. The values of k_{CS}, are found to be higher in more polar solvents in comparison to those in the nonpolar solvents (Table 2).

$$\Phi_{CS}=[(1/\tau_f)_{triad}-(1/\tau_f)_{ref}]/(1/\tau_f)_{triad} \qquad (2)$$

In view to observe the effect of concentration on the singlet state lifetime, we measure the fluorescence emission decay of TDPP (4) and BT-DPP-TPA (7) as a function of concentration in the range of from 4 μM to 1 mM of respective molecules by employing TCSPC with IRF 200 ps. Fig. 6 displays the typical change in fluorescence decays with time at around second vibronic peak of the emission band at 607 (see Fig.S5. & Fig.S6. for fluorescence decay at other wavelengths) and 670 nm for TDPP(4) and BT-DPP-TPA (7) respectively in varying concentration of 10 to 1000 μM. Both TDPP(4) and BT-DPP-TPA (7) exhibits predominantly monoexponential fluorescence decay. As shown in Fig.6A, singlet lifetime of TDPP(4) remains constant (~6.5 ns) till 50-60 μM of concentration and thereafter it starts increasing on increasing concentration. The singlet lifetime of TDPP(4) enhances to about 9.0 ns at 1 mM concentration.This increase of singlet lifetime can be attributed to static excimer formation of TDPP(4) in higher concentration regime. For BT-DPP-TPA (7) the change of singlet lifetime as a function of concentration is relatively smaller than that of TDPP(4) (Fig.6B). The singlet lifetime changes from 2.3 ns to 3.5 ns ongoing from 10 μM to 500 μM. These results reveal that due geometric constrains excimer formation is relatively weak in the triad system.

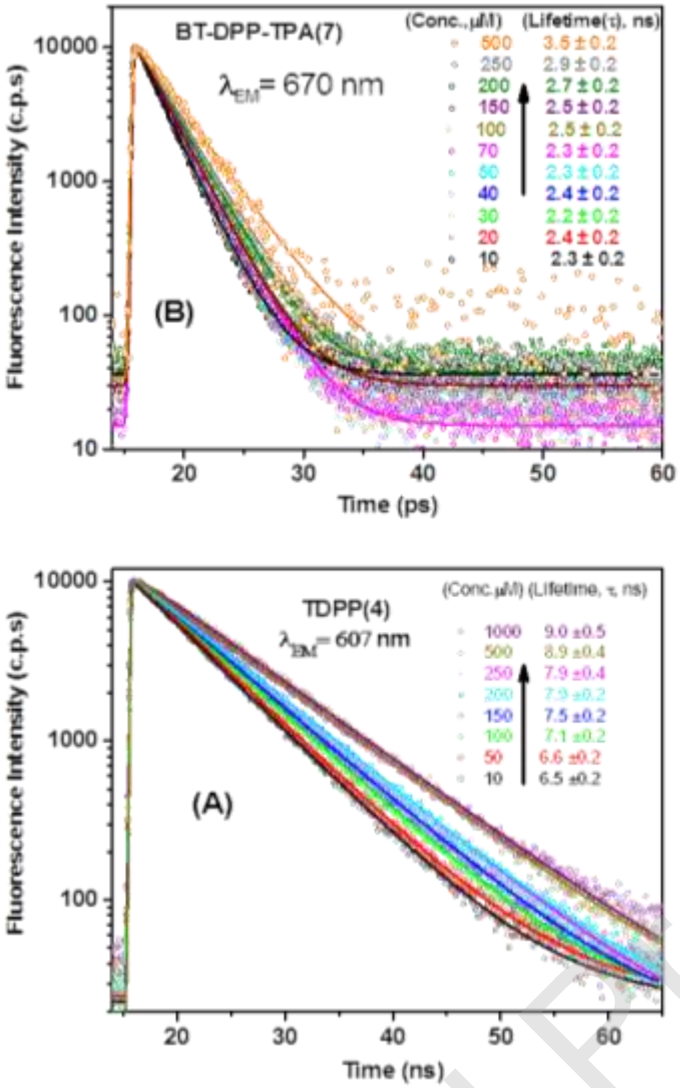

Fig.6. Fluorescence decays of TDPP(4) (A) and BT-DPP-TPA(7) (B) in different concentrations in chloroform solvent, λ_{Ex}= 400 nm.

3.2. Electrochemical Properties

The electrochemical properties of TDPP (4), TPA and BT-DPP-TPA(7) were investigated in DCM solvent using cyclic voltammetry (CV) to estimate the oxidation and reduction potentials of the triad and therefore to explore the thermodynamic feasibility of photoinduced electron transfer from TPA to singlet excited state of DPP in the triad. Fig. 7 represents the CV plots for TDPP(4), TPA, and BT-DPP-TPA(7). As shown in Fig. 7, TDPP(4) exhibits two quasi reversible oxidation processes and one reversible reduction process. The first oxidation potential of TDPP(4) is observed to 0.91V and the reduction potential is of -1.3V and TPA shows an oxidation potential 0.73 V. Upon attachment of TPA in BT-DPP-TPA(7), the oxidation process in triad becomes reversible in nature and shifts towards a negative potential (Fig. 7) whereas no noticeable change is observed in reduction process. This result indicates the direct interaction of TPA on the TDPP(4) derivatives and the influence of TPA to stabilize the radical cation and or radical anion during a redox reaction. The first oxidation potential of BT-DPP-TPA(7) is found to be 0.6 V. Based on observed E_{ox} and E_{red} potentials of the triad, thermodynamic free energy, the driving force of electron transfer from TPA moiety to exited DPP moiety for charge-separation ($-\Delta G_{CS}$) as well as charge-recombination ($-\Delta G_{CR}$) are estimated in all solvents using the eqs [55] as follow

$$\Delta G_{CS} = e(E_{OX} - E_{red}) - \Delta E^{S}_{0,0} + \Delta G_s \qquad (3)$$

$$\Delta G_{CR} = -e(E_{OX} - E_{red}) - \Delta G_s \qquad (4)$$

$$\Delta G_s = \frac{e^2}{4\pi\epsilon_0}\left(\frac{1}{2R_+} + \frac{1}{2R_-} - \frac{1}{R_{CC}}\right)\frac{1}{\epsilon_S} - \frac{e^2}{4\pi\epsilon_0}\left(\frac{1}{2R_+} + \frac{1}{2R_-}\right)\frac{1}{\epsilon_E} \qquad (5)$$

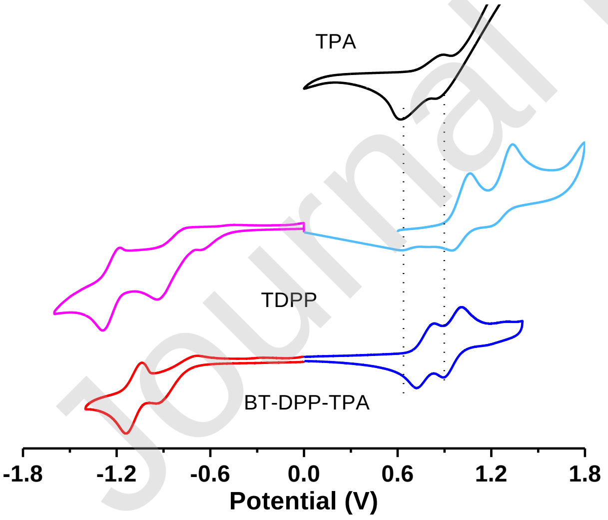

Fig. 7. Cyclic voltammogram of TDPP(4), BT-DPP-TPA(7) (1mM) in a DCM solution containing electrolyte 0.1 M, Tetrabutylammonium perchlorate (TBAP).

Table 1. Spectroscopic parameters of TDPP(4) and BT-DPP-TPA(7) (~10 µM) in different solvents

Solvent	Absorption				Emission				
	TDPP(4)		BT-DPP-TPA(7)		TDPP(4)		BT-DPP-TPA(7)		
	λ_{max} (nm)	ε_{max} x10^4 $M^{-1}cm^{-1}$	λ_{max} (nm)	ε_{max}x10^4 M^{-1} cm^{-1}	λ_{max} (nm)	τ (ns)	λ_{max} (nm)	τ (ns)	φ_{fl}
Hexane (2)	340	2.0 ± 0.5	346 ±2	1.9 ±0.5	560 ±2				
	356	1.70 ± 0.5	581 ±2	3.5± 0.5	603 ±2	6.5± 0.3	650 ± 2	2.6 ±0.3	0.1 ± 0.02
	508	4.2 ± 1.0	624 ± 2	3.8±0.5			702± 2		
	547	5.2 ±1.0	-----	---					
Chl (4.81)	341	1.9 ±0.5	349 ±2	2.2 ±0.5					
	357	1.7 ±0.5	592 ±2	3.7 ± 1.0	565 ± 2	6.5 ± 0.3	662 ± 2	2.3 ±0.3	0.08 ± 0.01
	512	3.6 ± 0.6	630 ±	4.0 ± 1.0	606 ± 2				
	548	4.1 ±1.0	------	------					
DMF (36.7)	341	3.6 ±0.6	346 ± 2	2.3 ± 0.5					
	354	3.2 ± 0.6	584 ± 2	4.0 ± 1.0	560 ± 2	6.5± 0.3	670 ± 2	1.8 ± 0.3	0.06 ± 0.01
	510	7.3 ± 1.0	624 ± 2	4.3 ± 1.0	600 ± 2				
	544	8.0 ± 1.0	----	-----					
ACN (37.5)	341	5.3 ± 1.0	345 ± 2	2.2 ± 0.6	560 ± 2				
	353	4.8 ± 1.0	585 ± 2	3.8 ± 0.6	600 ± 2		673 ± 2	---	0.03 ± 0.01
	508	10.0 ± 1.0	620 ± 2	4.0 ± 1.0					
	541	10.2 ±1.0	------	-----					
MeOH (32.7)	342	4.2 ± 1.0	346 ±22	2.3 ± 0.6	560 ± 2				
	355	3.8 ± 1.0	586 ± 2	3.9 ± 0.6	600 ± 2		675 ± 2	---	0.006 ± 0.002
	508	8.5 ± 1.0	616 ± 2	4.0 ± 0.6					
	536	8.6 ±1.0	-----	----					

where $\Delta E^{S}_{0,0}$ is the onset cross over point of absorption and fluorescence emission of TDPP(4) moiety in the triad and R_{+}, R_{-}, and R_{CC} are radii of TPA and DPP and centre-to-centre distance between donor and acceptor respectively, and e, ε_0, are the electronic charge, vacuum permittivity, ε_S and ε_E dielectric constant of solvent used for spectroscopic measurement and electrochemical measurements respectively. Accounting the value of R_{+}, R_{-} and R_{cc} obtained from optimized geometry employing DFT calculation (see ESI for more, Fig. S7.), which are of the order~5Å and ~7Å respectively, the ΔG_{CS} and ΔG_{CR} are calculated and they are listed in Table 2. The ΔG_{CS} values are found to be negative in all solvents whereas it is near to zero in hexane. These results suggest that the formation of photoinduced charge-separated (CS) state upon excitation to DPP moiety in the triad is exergonic in nature indicating CS reaction is an energetically downhill and spontaneous process in reductive pathways. Note, BT moiety of BT-DPP-TPA(7) is also considered to be a donor with very weak electron donating ability. The oxidation potential of BT derivatives is expected to be very high (E_{ox}=1.8 V vs SCE) [56] and no oxidation peak was appeared in voltammogram of BT-DPP-TPA(7) in the observation window of 2 V. Hence, the possibility of photoinduced electron transfer process from BT moiety to excited DPP moiety in BT-DPP-TPA(7) is ruled out.

3.3. Femtosecond Transient Absorption Spectra

To understand the thorough insight of relaxation dynamics of BT-DPP-TPA(7) and probable photoinduced reaction dynamics we extend our quest by carrying out femtosecond transient absorption (*fs*TA) studies for TDPP(4) and BT-DPP-TPA(7) in nonpolar and polar solvents. First, we carried out *fs*TA studies of TDPP(4) upon S_2 excitation at 340 nm in different solvents probing in the range from 520 to 765 nm (the extreme limit of our spectrometer) and explored the spectrotemporal information of relaxation mechanism. Then we performed exactly similar types of *fs*TA studies for BT-DPP-TPA(7) and reveal the role of TPA in BT-DPP-TPA(7) as an electron donor. Fig. (8) illustrates a typical profile diagram of *fs*TA studies of TDPP(4) in chloroform which consists of elite ΔOD heat map, TA spectra at particular delay times, and time traces at different wavelengths. TA spectra are well positioned corresponding to the ground state bleaching (GSB), stimulated emission (SE), and excited state absorption (ESA). Immediate after excitation, a negative signal pertaining to GSB, SE (blue color in Fig. 8a_1) appeared over the range of 520−650 nm region. In addition to these strong negative signals, a spontaneous rise of very broad positive signal (ESA) (red color, Fig. 8a_1) above 650 nm appears with no specific peak in the studied spectral wndow. This positive signal observed at the very initial stage is assigned to be $S_n \leftarrow S_2$ transition. However, within a few ps of delay

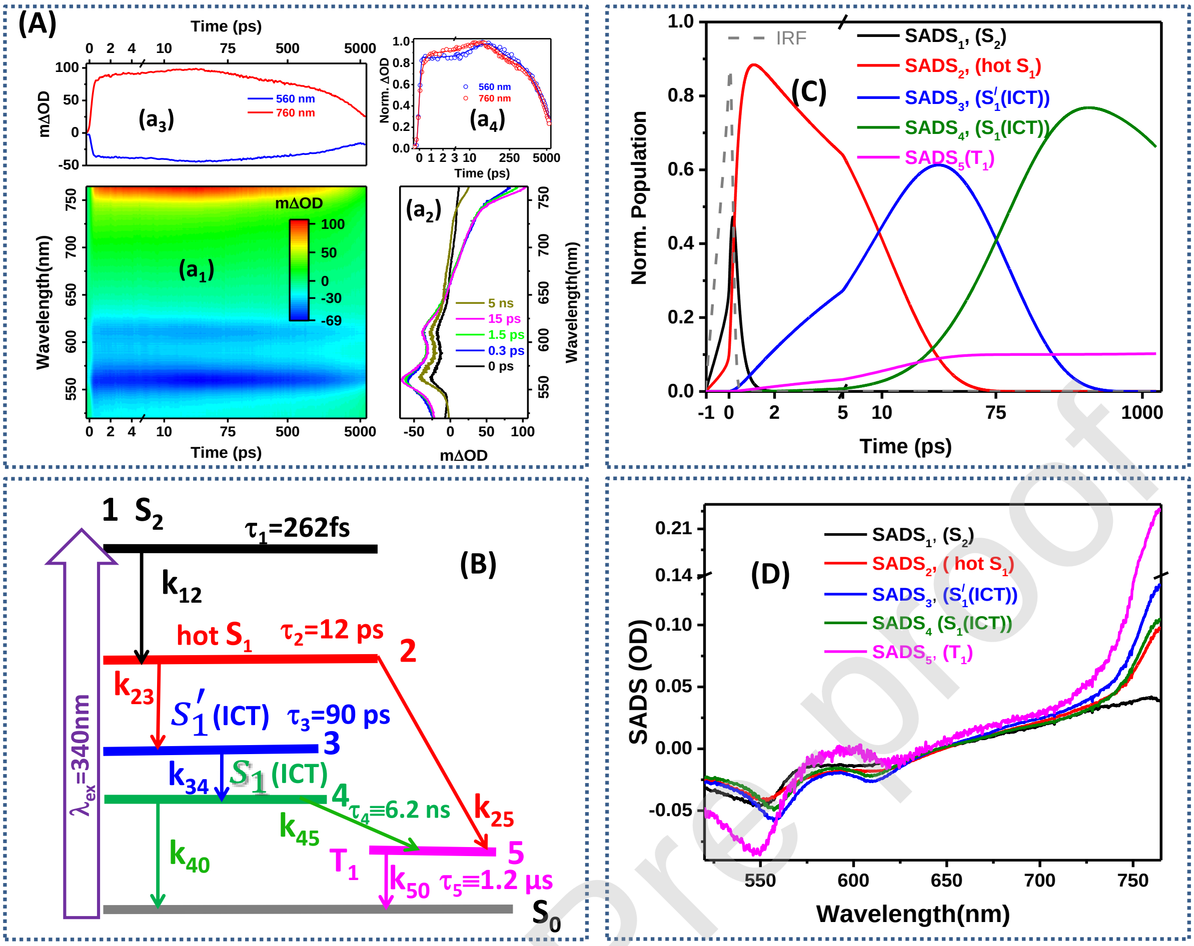

Fig. 8. Pictorial summary of *fs*TA study of TDPP(4) upon 340 nm excitation in Chloroform solution (0.1 mM). (A) Profile picture of *fs*TA: ΔOD heat map, blue colour indicates negative signals (GSB/SE), red indicates positive(ESA) and greenish blue to green indicates zero level (a_1), TA spectra at selected time delays (a_2), time traces at two different wavelengths (a_3) and normalised time traces of GSB, SE and ESA at 560 and 760 nm respectively (a_4). Time trace at 560 nm is inverted to positive values for easy comparison with positive signal at 760 nm. (B) Five levels (states) kinetic target mode used for global fitting. Rate of depopulation of S_2, k_{12}= (262fs)$^{-1}$, rate of IC; rate of depopulation of hot S_1 consists of rate of IC, k_{23}= 0.90x(12 ps)$^{-1}$; rate of SF k_{25}= 0.10x(12ps)$^{-1}$; rate of IC of $S_1^{'}$(ICT), k_{34}=(90 ps)$^{-1}$; rate of depopulation of S_1(ICT), k_{40}=0.95x(6.2 ns)$^{-1}$; rate of ISC, k_{45}=0.05x(6.2 ns)$^{-1}$. (C) & (D) represent the spectrotemporal picture resulted from target based global analysis. Normalized population profiles of corresponding to five states (C), SADSs spectra of corresponding to five states (D). Time axis is linear till 5ps and thereafter it is logarithmic scale.

time, this positive signal becomes narrow and gets blue shifted to have a peak position apparently at 760 nm. Furthermore, the intensity of this positive signal increases with delay time for a few ps. This later time positive signal is assigned to $S_n \leftarrow S_1$ transition of TDPP(4)

[40,41]. The spectral shape and the time evolution are shown in Fig. 8a$_2$ and Fig 8a$_3$ respectively. Fig. 8a$_4$ shows the normalized time traces of GSB/SE signals and ESA signals at 560 and 760 nm respectively. For the easy comparison of the time evolution of GSB/SE signal to that of ESA signal, GSB/SE signal is inverted. As shown in Fig. 8a$_4$, a distinct recovery of GSB/SE signal is closely associated with the rise of ESA at 760 nm in the very early time of spectral evolution. These results are primarily linked to the deactivation of S_2 state to hot S_1 state. Followed by this, nearly similar kinds of rise of GSB/SE and ESA signals are observed in few ps time domain at 560 and 760 nm respectively. This can be rationalized to subsequent thermal and structural relaxation of hot S_1 state to S_1 state. Finally, to our surprise, a relatively slow rise both in GSB/SE signal at 560 and ESA signal at 760 nm are observed in few tens of ps time scale followed by recovery dynamics of GSB/SE which is similar to the decay dynamics of ESA signals at 760 nm (Fig. 8a$_4$). Therefore, five exponential functions with 200-300fs, 10-50 ps, 50-200 ps, 5000-6000 ps and a very slow component with large time constants are essential to fit these time traces satisfactorily. Since the molecule was excited at S_2 state, the first component could associate with the lifetime of S_2 state and the second component can be assigned as the lifetime of hot S_1 state. In accordance with the literature [22,57,58] the third component is assigned to the unrelaxed intramolecular charge transfer state $S_1^{'}(\mathrm{ICT})$ which structurally relaxes to S_1(ICT) by virtue of planarization of the thiophene donor to the DPP core acceptor [58]. The fifth long-lived component is attributed to the lifetime of the triplet state. It is important to note here that the observed increase of the GSB signal in 50-200 ps time domain is associated with the fact of depletion of the ground state population and it can be correlated with the increase of triplet state population due to singlet fission, SF ($S \rightarrow TT$), in the hot S_1 state. In the same way, the increase of ESA signal at 50-200 ps time scale above 750 nm corresponds to $T_n \leftarrow T_1$ absorption resulting from

SF. Note, the strong signal pertaining to $T_n \leftarrow T_1$ transitions of TDPP is reported elsewhere to be in the region of 750 to 1000 nm [59]. However, the increase of GSB signal with delay time accompanied by an increase of ESA ($T_n \leftarrow T_1$) signal above 750 nm is eventually assigned as the signature of singlet fission. Note, Wasielewski and co-workers reported singlet fission phenomena in DPP derivatives in solid-state exciting at 515 nm, a blue end of S_1(ICT) absorption of TDPP derivatives [22,58]. However, they did not observe SF in DPP derivatives in the solution phase upon 550 nm excitation, at the peak of the S_1 absorption band. Indeed, initially, we also failed to observe this increase of GSB on increase in delay time and increase of ESA signal above 750 nm when TDPP (4) ([TDPP]<100 μM) was excited in the vicinity of S_1 absorption maxima at around 500nm. It is important to mention here that we perform *fs*TA studies with a quartz cell of 1 mm optical path length and adjust the concentration of the solution in such a way that optical density at the wavelength of excitation becomes less than 0.5. Further to be noted, the molar extinction coefficient of the S_1 band of TDPP(4) at 500 nm is more than twice time higher than that of the S_2 band at 340 nm. Hence, *fs*TA studies exciting at S_2 band (340 nm) are performed in higher concentrations than *fs*TA studies performed upon excitation at 500 nm. Therefore, the minimum concentration of TDPP(4) employed for *fs*TA study upon 340 nm excitation is calculated to be ~0.10 mM, whereas the minimum concentration employed for *fs*TA study upon 500 nm is <0.10 mM and we observed neither the increase in GSB signal nor the rise of ESA signal on the delay time in 50-200 time window. This result clearly indicates that concentration plays a role in observing the enhancement of GSB on the delay time. Furthermore, concentration dependent *fs*TA studies (Fig. S8a) confirm that the traceable increase of GSB signal in 50-200 ps (delay) time window started appearing on 0.1 mM concentration of TDPP(4) and above 0.10 mM of concentration it becomes more prominent (Fig. S8b). These results clearly indicate that SF

(S→TT) occurs in a higher concentration regime when aggregation occurs in the ground state.

Concentration dependent studies of steady state absorption, fluorescence emission and time resolved fluorescence emission showed the propensity of aggregate formation in the ground state of TDPP(4) in higher concentration (preferably above 60-70 µM). Hence photo-excitation of TDPP(4) solution above 100 µM (0.1 mM) concentration could lead to form static excimer like an intermediate between one photoexcited and one ground state molecule which may produce correlated multiexciton $^1(T_1T_1)$ that leads formation of the uncorrelated triplet excitons. In addition to this, in higher concentration possibility of formation of excimer like intermediate state (dynamic excimer) via diffusive encounters of ground state molecules to the photo-excited molecules generating two triplets excitations can not be completely ruled out. For both the instances (static and dynamic excimers), the intermediate disappears when two triplets separate into two TDDP(4) molecules which in turn increases the GSB on the delay time. Hence, we attribute this increase of GSB signal at 50-200 ps time window to SF and it occurs only in a relatively higher concentration regime of TDDP(4). However, a more planned and systematic studies are essential to unveil the exact mechanism of SF formation of TDPP(4) and its derivatives in solution phase and we plan it soon.

Table 2. Free energy for charge separation, charge recombination, rate constants for charge separation (k_{CS}), rate constants charge recombination (k_{CR}), and quantum efficiency of charge separation in different solvents

Solvent	$-\Delta G_{CS}$	$-\Delta G_{CR}$	Φ_{CS}(%)	k_{CS}x10^8s^{-1}	k_{CR}x10^8 s^{-1}
Hexane	-0.02	1.97	59	2.26 (2.38)	(~0.2)
Chl	0.19	1.73	64	2.76 (3.06)	(~0.05)
DMF	0.33	1.57	71	3.97 (4.50)	(~0.1)
ACN	0.35	1.57	----	---	---
MeOH	0.34	1.58	---	---	---

Rate constants values are in parenthesis obtained from global analysis of TA data and without parenthesis obtained from TCSPC data

Based on these observations a minimum of five levels/states kinetic target model with minimum number of branching of each level/state (Fig.8B) is essential to fit the whole *fs*TA data matrix globally estimating the precise values of kinetic parameters. In five levels/states kinetic target model (Fig.8B), the first state corresponds to S_2 as the most of the excitation energy (λ_{Ex}=340 nm) was deposited to S_2 state and it hastily relaxed to hot S_1 (second state) by internal conversion with rate constant k_{12}. The hot S_1 state plays a major role in the deactivation process of TDPP(4) and it decays through a minimum of two distinct channels populating two different states: first, it goes to structurally unrelaxed intramolecular charge transfer state $S_1'(\mathrm{ICT})$ via internal conversion, and second, it populates triplet state through SF process with rate constants k_{24} and k_{25} respectively. The third state which is very typical state of DPP derivatives [21,22,57] i.e. unrelaxed $S_1'(\mathrm{ICT})$ state decays to structurally relaxed S_1 (ICT) state, the fourth state of the model, with rate constant k_{34} and S_1 (ICT), predominantly depopulates to ground state (S_0) and very slowly to triplet state (T_1) via intersystem crossing with rate constants k_{40} and k_{45} respectively. Finally, the fifth state i.e. the triplet state which very slowly decays to S_0 with rate constant $k_{50.}$ The proposed model nicely replicated the experimentally observed *fs*TA data (goodness of the fit shown in Fig. S9) and justifies the undergoing relaxation process of photoexcited TDPP(4).

The extracted lifetime values of each state are shown in Fig.8B. Fig. 8C and Fig 8D show the spectrotemporal behaviors of TDPP(4) arising out of this fit to the proposed kinetic target scheme with normalized population profiles, the time evolution of the respective states, and species associated difference spectra (SADSs), the spectral signature of the respective states. The $SADS_1$, $SADS_2$ $SADS_3$, $SADS_4$, and $SADS_5$ signify the state of S_2, hot S_1, $S_1'(\mathrm{ICT})$, S_1(ICT), and T_1 states respectively. The lifetime of $SADS_1$ (S_2), $SADS_2$ (hot S_1), $SADS_3$, and $S_1'(\mathrm{ICT})$ are found to be 0.26, 12, and 90 ps respectively. The lifetime of $SADS_4$ (S_1(ICT)) was kept to the constraint of fit to the value (~6 ns) obtained in TCSPC method. Similarly, the lifetime of $SADS_5$(T_1) was fixed to 1-2 μs which is too large to estimate from 5-6 ns time window data. However, the lifetime value of this level does not affect the lifetime values of higher energy levels. The fitting of the proposed target model estimates that 90 and 10% of population of hot S_1 goes to $S_1'(\mathrm{ICT})$, and T_1 respectively. The transfer of 10% population of hot S_1 to triplet state is due to SF process, one single molecule generates two correlated triplet state molecules ($S \rightarrow TT$), and the k_{25} is rate of SF (k_{SF}) which is calculated to be 12.5×10^9 s^{-1} and this in turn predicts the SF time ($\tau_{SF}=1/k_{SF}$) to be 120 ps. Exactly, similar kinds of relaxation mechanism of TDPP(4) is also observed in nonpolar hexane solvent.

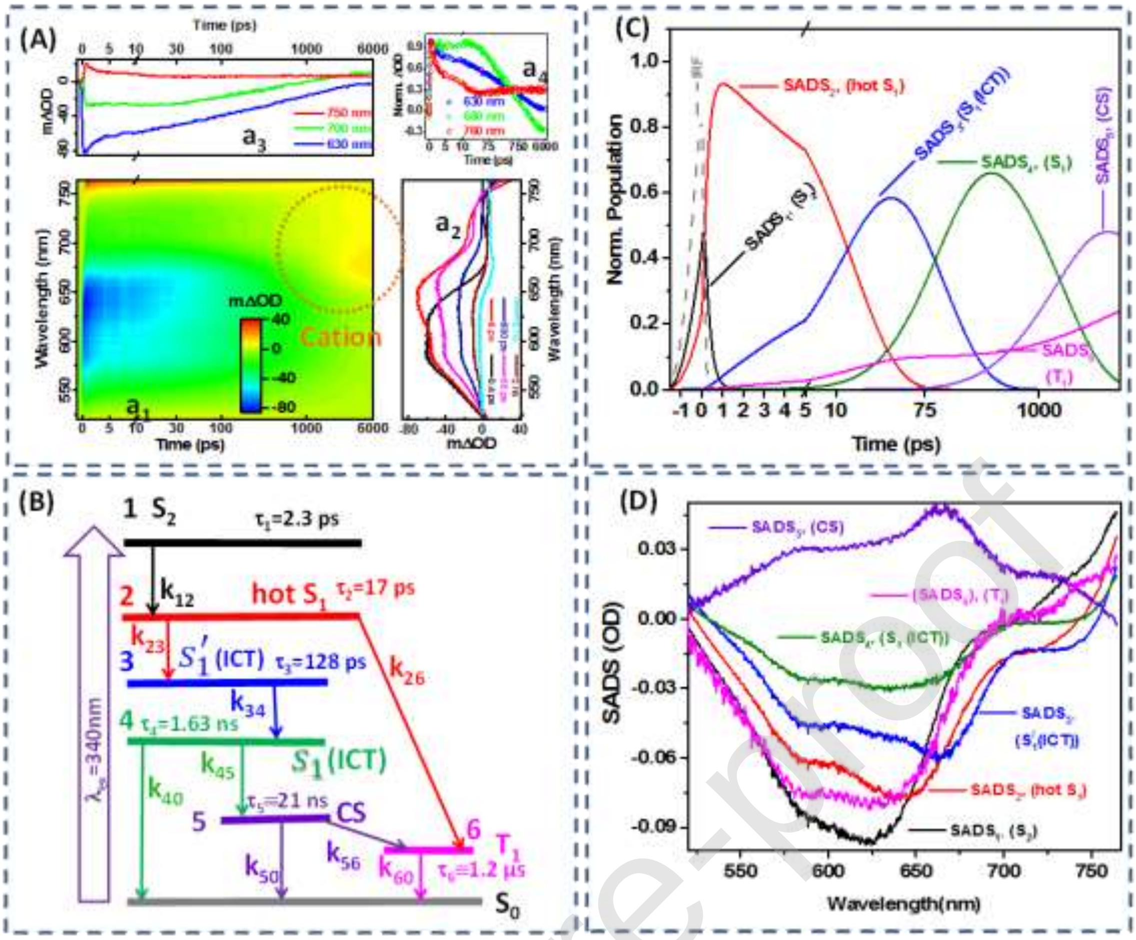

Fig. 9. Pictorial summary of *fs*TA study of BT-DPP-TPA(7) upon 340 nm excitation in chloroform solution (0.1mM). (A) Profile picture of *fs*TA: ΔOD heat map, blue colour indicates negative signals(GSB/SE), red indicates positive (ESA) and greenish yellow indicates zero level (a_1), TA spectra at selected time delay (a_2), time traces at three different wavelengths (a_3) and normalised time trace of GSB,SE and ESA at 630, 680 and 760 nm respectively (a_4). Time trace at 630 and 680 nm are inverted to positive values for easy comparison with positive signal at 760 nm. (B) Six levels (states) kinetic target model used for global fitting. Rate of depopulation of S_2, $k_{12}=(2.3\text{ps})^{-1}$(IC); rate of depopulation of hot S_1, rate of IC, $k_{23}=0.9 \times (17\text{ps})^{-1}$; rate of SF, $k_{26}=0.1\text{x}(17\text{ps})^{-1}$; rate of IC of $S_1^{\prime}$(ICT), $k_{34}=(128\text{ps})^{-1}$; rate of depopulation of S_1 (ICT) to S_0 , $k_{40}=0.40\text{x}(1.63\text{ ns})^{-1}$; rate of CS, $k_{45}=0.60\text{x}(1.63\text{ ns})^{-1}$; rate of direct charge recombination(CR), $k_{50}=0.6\text{x}(21\text{ ns})^{-1}$; rate of charge recombination(CR) via triplet, $k_{56}=0.4\text{x}(21\text{ ns})^{-1}$ (C) & (D) represent the spectrotemporal picture resulted from target based global analysis. Normalized population profile of corresponding to six states (C), SADS spectra of corresponding to six states (D). Time axis is linear till 5ps and thereafter it is logarithmic scale.

After exploring the relaxation mechanism of TDPP(4) we performed *fs*TA studies for BT-DPP-TPA(7) upon S_2 excitation in different solvents. Fig. 9 illustrates a comprehensive summary of the *fs*TA study of BT-DPP-TPA(7) in chloroform solution upon 340 nm excitation. The profile picture of *fs*TA study (Fig. 9A) consisting of elite ΔOD heat map, TA spectra at different delay times, and time traces at different wavelengths feature the time evolution of transient absorption. As can be evidently seen (Fig. 9A), transient absorption is composed of superposition of GSB, SE, (ΔOD<0, green to blue colors in heat map) corresponding to ground state absorption and fluorescence emission and ESA (yellow to red in heat map) in the studied spectral range. In the early delay stage, the time evolution of transient absorption of BT-DPP-TPA(7) is almost parallel to that of TDPP(4). Likewise TDPP(4), instead of the recovery of GSB signals a rise in GSB signal is observed in few ten of picosecond time domain (Fig. 9A (a_4)) along with a distinct rise in same time scale in ESA signal above 750 nm which are regarded as the signature of SF process. However, the most discriminatory feature of transient absorption spectra of BT-DPP TPA(7) with respect to that of TDPP(4) is found to be the appearance of a positive signal above 650 nm at later stage of delay time and this new positive signal is attributed to the absorption of TPA radical cation [60,61]. Hence, this result is combined with the fact of electron transfer reaction from TPA to photoexcited DPP moiety in BT-DPP-TPA(7). However, due to the superposition and interplay of a negative and positive signal of TA spectra pertaining to GSB, SE, ESA, DPP^{-} and $TPA^{+\cdot}$ radical cation [60,61] respectively in the same spectral window, the time traces at different wavelengths (Fig. 9 a_4) are too critical to fit by multiexponential functions. The whole TA data matrix is globally analyzed with six levels/states kinetic target model with a minimum number of possible branching of each state. Fig. 9B shows the target model used to fit the TA data matrix of BT-DPP-TPA(7). As shown in the target model, the relaxation pathways for the first four levels are exactly similar and a new level/state is introduced in order to accommodate the ET reaction forming charge separated state (CS) energetically placing in between S_1 and T_1. Note, the thermodynamic free energy for CS formation ($-\Delta G_{CS}$) is in the order of ~0.3 eV (Table 2) which assures that CS state lies between S_1 and T_1 in BT-DPP-TPA(7). Considering the energetic position of CS state, we propose that charge recombination (CR) occurs through two channels: firstly, it recombines to ground state (k_{50}), and secondly it recombines to T_1 (k_{56}) state via rate limiting intersystem crossing to triplet CS state. Based on this kinetic target model TA data are nicely reproduced (Fig. S10) yielding SADSs (Fig. 9C) corresponding to each state with their respective population profiles (Fig. 9D) along with estimated microscopic rates (Fig. 9B) and they are shown in Fig. 9. Likewise in TDPP(4), the $SADS_1$, $SADS_2$, $SADS_3$, and $SADS_4$ represent S_2, hot S_1, S_1'(ICT) and S_1 (ICT) states respectively with nearly similar kinds of lifetime values and they are 2.3, 17, 128, and 1630 ps respectively. The rate constant k_{26}, i.e. the rate of SF process (k_{SF}), is calculated to be 5.9×10^9 s^{-1} which in turn suggests that SF takes place in 170 ps ($\tau_{SF}=1/k_{SF}$) in BT-DPP-TPA(7). The $SADS_5$ represents the CS state which is found to be avery broad spectra consisting aparently of three absorption peaks at ~575,~675 and ~730 nm which are assigned to be the absorption band of DPP^- anion and $TPA^{+\cdot}$ cation radical respectively [61,62]. The rate constant ($k_{CS}=k_{45}$) of CS state formation is estimated to be 3.06×10^8 s^{-1} which indicates that the formation time of CS state is to be 2.2 ns. The lifetime of CS state is found to be very long and it can be assumed ~21 ns as it is too long to detect from the data of 6 ns time window and this value was treated as the constraint of fit. Therefore, the rate of charge recombination ($k_{CR}=k_{50}+k_{56}$) be approximately estimated to be ~ $5 \times 10^7 s^{-1}$ and it is found to be, at least, one order slower than the rate of charge separation. Transient absorption studies in hexane, a nonpolar solvent (Fig. S11. & Fig.S12) and DMF, a strongly polar solvent (Fig. S13) show similar kinds of results and rate of CS formation found to be increasing on going from nonpolar to polar solvents and they are placed in table 2. To our surprise, the rate of charge recombination in hexane is estimated to be faster than that of in more polar medium (Table 2). This unusual behavior of CR rate could be due to asymmetrically designed push-pull type triad, a feature that was not evident in the push-pull type of triads constructed using symmetric TPA as electron donors [60]. The exact role of BT in BT-DPP-TPA (7) in the formation of CS state is not known. However, BT moiety with rigid structure and very weak electron donating ability could minimize the steric hindrance and enhance the planarity of the molecule in favour of electron transfer reaction from TPA to DPP core. Furthermore, in nonpolar medium easy formation of static excimer lead to facial SF which could play a role in determining CS and CR rates in the solvents of different polarities.

4. Discussion

Singlet fission is a spin allowed process although it produces excited triplets (scheme 1) from excited state. Hence, it is regarded as a special case of internal conversion which is very fast in nature. Therefore, when the energetic criterion is satisfied and the intermolecular coupling between two molecules is favorable, SF occurs on a very short time scale, often competing with vibrational cooling and outcompeting radiative fluorescence emission [24]. The report of SF in homogeneous solution, especially for molecules with a single chromophore, is very rare although it is feasible in solution phase for higher concentration of ground state molecules such that either tendency of aggregate formation increases or diffusive (S_1+S_0) encounters become too large. As discussed before SF was reported for TDDP (4) in film employing *fs*TA studies [22] but it was overlooked by Mauck et al [22] in solution phase perhaps due to two reasons: first, they had performed *fs*TA studies at low concentration (OD~0.2 at 550 nm $\approx$ few µM of concentration) in which formation of ground state aggregation did not occur or it did not generate frequent diffusive encounters between S_1 and S_0 molecules forming excimer like complexes, a necessary condition for SF. Secondly, in the solution phase, they had pumped the molecule at 550 nm, red edge of ground state absorption spectra which may not exactly satisfy energetic criteria ($E(S_1) \geq 2E(T_1)$) as singlet fission does not essentially occur from relaxed S_1 state without necessary thermal activation[24]. As describes (*vide supra*), in our *fs*TA studies, we observed a distinct rise of GSB and increase of ESA signal above 750 nm in 50-200 ps time window when the concentration of TDPP(4) or BT-DPP-TPA(7) was above 0.1mM and it is assigned as the signature of SF in these studied systems. Owing to very high fluorescence quantum yield, the population of T_1 state of TDPP(4) by intersystem crossing is very slow and $T_n \longleftarrow T_1$ transition is seldom observed in *fs*TA studies. Here we have identified species associated difference spectra ($SADS_5$) of $T_n \longleftarrow T_1$ transition for TDPP(4) in 500-750 spectral window (750 nm is the limit of our spectrometer for the present *fs*TA set up) which very closely resembles the reported spectra for DPP derivatives observed nanosecond laser flash photolysis experiment. Similarly, $T_n \longleftarrow T_1$ transition ($SADS_6$) is also observed due to SF in BT-DPP-TPA(7). Note, Pun et al. had shown that aryl substitution on pyrrole nitrogen of DPP lowered the singlet energy substantially, whereas, lowering of triplet state energy was not that extent (the DPP triplet energy is 1-1.15 eV as reported) which helped triplet fusion to occur [28] but same criterion does not necessarily satisfy SF to occur from lowest singlet energy of DPP. For thermodynamically favourable SF, the lowest triplet excited state energy of the probe molecule must be less than or equal to half of its lowest singlet excited state energy. Likewise TDPP(4) observation of rise of ground state bleaching in TA studies of BT-DPP-TPA(7) along with increase of ESA signal in 50-200 ps time domain confirms the occurrence of SF in BT-DPP-TPA(7). This result complies with the thermodynamic criterion of SF in BT-DPP-TPA(7). In our *fs*TA studies, we have pumped both the systems either 340 nm, S_2 state of both the molecules or 515 nm and 550 nm, the blue end of S_1(ICT) state of TDPP(4) and BT-DPP-TPA (7) respectively. Hence, in all the cases a sufficient amount (0.3-0.45 eV≈1818-

3250 cm^{-1}) of excess energy was deposed to the system populating hot S_1 state and it eventually satisfies the adiabatic energy criteria for ($S_1 \geq 2T_1$) especially in BT-DPP-TPA (7) system.

In addition to SF process, CS process occurs in BT-DPP-TPA(7) triad in longer time domain and it is relatively slower than SF process. The CS and CR dynamics are exactly similar to that of in lower concentration of BT-DPP-TPA(7) triad molecule when no trace of SF is detected. Even, in higher concentration of BT-DPP-TPA(7), where the aggregation is expected in ground state may contribute charge separation across the multiple molecules. Furthermore, SF and CS are independent phenomena and the molecule which takes part in SF does not take part in CS process as CS is a very slow process in the studied triad system. In higher molar concentration of BT-DPP-TPA(7), SF occurs in the case of favorable static excimer formation for which proper orientations of excited DPP moiety and one ground state DPP moiety are satisfied. Hence SF does not interfere in the CS process at all.

5. Conclusion

In summary, we have successfully synthesized and photo physically characterized a push–pull triad molecule (BT-DPP-TPA(7)) comprising diketopyrrolopyrrole, triphenylamine, benzothiophene and thiophene. The triphenylamine, benzothiophene and diketopyrrolopyrrole entities owing to facile redox potentials produced higher exothermicity favoring the formation of a relatively faster photoinduced charge separation process and slow charge recombination process. Upon photoexcitation, to DPP moiety of BT-DPP-TPA(7) reductive photoinduced electron transfer occurs from ground state TPA to excited singlet state of DPP leading to the CS process. Apart from this event, we demonstrate for the first time that both TDPP(4) and BT-DPP-TPA(7) take part in SF in the solution phase in 100-200 ps time scale for the solution of the concentration on and above 100 μM. The rate of charge separation, k_{CS}, is found to be (10^9–10^8 s^{-1}) and it increases on going from nonpolar to polar medium. The rate of charge recombination, k_{CR}, was found to be extremely slow (ns time scale) in all solvents. Hence, we demonstrated that upon photo-excitation as prepared BT-DPP-TPA(7) triad generates long-lived CS state and also undergoes SF process acting as SF sensitizer. These combined rare features in BT-DPP-TPA(7) may have implications for improving the efficiency of photovoltaic devices using DPP derivatives.

Electronic Supplementary Information (ESI†)

Additional absorption and fluorescence emission spectra of TDDP(4) and BT-DPP-TPA (7) in different solvents, concentration dependent absorption spectra of TDDP(4) and BT-DPP-TPA (7) in chloroform, ground state optimized geometry of BT-DPP-TPA (7), concentration dependent TA spectra, ground state bleaching recovery dynamics showing SF for TDPP(4), global and target analysis results showing the goodness of fit, transient absorption spectra and global and target analysis of triad in hexane, ^{1}H-NMR and MALDI-MS spectra of BT-DPP-TPA (7).

Authors statements

Please find enclosed revised (PHOTOCHEM-D-20-00847) manuscript entitled " *Charge Separation and Singlet Fission in Covalently Linked Diketopyrrolopyrrole Derivatives and*

Triphenylamine Triad in Solution" based on our recent research work done by Madhu Chakali(graduate student), Haraprasad Mandal(graduate student), Munisamy Venkatesan(graduate student), Bharath Dyaga(postdoc), V. Jayathirtha Rao(emeritus scientist), Prakriti Ranjan Bangal (principal Scientist) in favor of publication in your esteemed journal J. Photochem. Photobiol A: Chem. The manuscript has been revised after performing more experiments in the light of reviewers concerned and changes made in the manuscript are highlighted for your convenience. We also assure that not a single portion of this manuscript has not been submitted elsewhere for publication.

Conflict of interest

There is no conflict of interest

Acknowledgments

We thank Director CSIR-IICT for the support (IICT/Pubs./2019/371). MC, MV thank

CSIR and HM thanks to UGC for providing a research fellowship.

References

[1] Z. Hao, A. Iqbal, Some aspects of organic pigments, Chem. Soc. Rev., 1997, 26, 203–213.

[2] O. Wallquist, R. Lenz, 20 Years of DPP Pigments-Future Perspectives, Macromol. Symp., 2002, 187, 617–629.

[3] O. Wallquist In High-Performance Pigments; Ed. M. H. Smith, Wiley-VCH: Weinheim, 2002, 159-184.

[4] B. Walker, C. Kim and T.-Q. Nguyen, Small Molecule Solution-Processed Bulk Heterojunction Solar Cells, Chem. Mater., 2011, 23, 470–482.

[5] M. Fukuda, K. Kodama, H. Yamamoto and K. Mito, Solid-state laser with newly synthesized pigment, Dyes Pigm., 2002, 53, 67–72.

[6] M. Fukuda, K. Kodama, H. Yamamoto and K. Mito, Evaluation of new organic pigments as laser-active media for a solid-state dye laser, Dye. Pigment., 2004, 63, 115–125.

[7] J. Tang, W. J. Wu, J. L. Hua, J. Li, X. Li and H. Tian, Starburst triphenylamine-based cyanine dye for efficient quasi-solid-state dye-sensitized solar cells, Energy Energy Environ. Sci., 2009, 2, 982.

[8] K. Sayama, K. Hara, Y. Ohga, A. Shinpou, S. Suga and H. Arakawa, Significant effects of the distance between the cyanine dye skeleton and the semiconductor surface on the photoelectrochemical properties of dye-sensitized porous semiconductor electrodes New J. Chem., 2001, 25, 200-202.

[9] X. Ma, J. Hua, W. Wu, Y. Jin, F. Meng, W. Zhan and H. Tian, A high-efficiency cyanine dye for dye-sensitized solar cells, Tetrahedron, 2008, 64, 345-350.

[10] A. C. Khazraji, S. Hotchandani, S. Das and P. V. Kamat, Controlling Dye (Merocyanine-540) Aggregation on Nanostructured TiO2 Films. An Organized Assembly Approach for Enhancing the Efficiency of Photosensitization, J. Phys. Chem. B, 1999, 103, 4693-4700.

[11] K. Sayama, K. Hara, N. Mori, M. Satsuki, S. Suga, S. Tsukagoshi, Y. Abe, H. Sugihara and H. Arakawa, Photosensitization of a porous TiO2 electrode with merocyanine dyes containing a carboxyl group and a long alkyl chain, Chem. Commun., 2000, 1173-1174.

[12] Z. S. Wang, Y. Cui, Y. Dan-oh, C. Kasada, A. Shinpo and K. Hara, Thiophene-Functionalized Coumarin Dye for Efficient Dye-Sensitized Solar Cells: Electron Lifetime Improved by Coadsorption of Deoxycholic Acid, J. Phys. Chem. C, 2007, 111, 7224-7230.

[13] K. Hara, K. Sayama, Y. Ohga, A. Shinpo, S. Suga and H. Arakawa, A coumarin-derivative dye sensitized nanocrystalline TiO2 solar cell having a high solar-energy conversion efficiency up to 5.6% , Chem. Commun., 2001, 569-570.

[14] E. Stathatos and P Lianos, Synthesis of a hemicyanine dye bearing two carboxylic groups and its use as a photosensitizer in dye-sensitized photoelectrochemical cells, Chem. Mater., 2001, 13, 3888-92.

[15] Z. S. Wang, F. U. Li and C. H. Huang, Highly efficient sensitization of nanocrystalline TiO2 films with styryl benzothiazolium propylsulfonate, Chem. Commun., 2000, 2063.

[16] T. Horiuchi, H. Miura and S. Uchida, Highly-efficient metal-free organic dyes for dye-sensitized solar cells, Chem. Commun., 2003, 3036-3037.

[17] T. Horiuchi, H. Miura, K. Sumioka and S. Uchida, High Efficiency of Dye-Sensitized Solar Cells Based on Metal-Free Indoline Dyes, J. Am. Chem. Soc., 2004, 126, 12218-19.

[18] S. Qu and H.Tian, Diketopyrrolopyrrole (DPP)-based materials for organic photovoltaics, Chem. Commun., 2012, 48, 3039–3051

[19] B. Yadagiri, K. Narayanaswamy, R. Srinivasa Rao, A. Bagui, R. Datt, V. Gupta and S. P. Singh, D−π−A−π−D Structured Diketopyrrolopyrrole-Based Electron Donors for Solution-Processed Organic Solar Cells, ACS Omega, 2018, 3, 13365−13373.

[20] S. Qu, W. Wu, J. Hua, C. Kong, Y. Long and H. Tian, New Diketopyrrolopyrrole (DPP) Dyes for Efficient Dye-Sensitized Solar Cells, J. Phys. Chem. C, 2010, 114, 1343–1349.

[21] C. M. Mauck, P. E. Hartnett, Y. L. Wu, C. E. Miller, T. J. Marks and M. R. Wasielewski, Singlet Fission within Diketopyrrolopyrrole Nanoparticles in Water, Chem. Mater., 2017, 29, 6810−6817.

[22] C. M. Mauck, P. E. Hartnett, E. A. Margulies, L. Ma, C. E. Miller, G. C. Schatz, T. J. Marks and M. R. Wasielewski, Singlet Fission via an Excimer-Like Intermediate in 3,6-Bis(thiophen- 2-yl)diketopyrrolopyrrole Derivatives, J. Am. Chem. Soc., 2016, 138, 11749−11761.

[23] A. M. Levine, C. Schierl, B. S. Basel, M. Ahmed, B. A. Camargo, D. M. Guldi and A. B. Braunschweig, Singlet Fission in Combinatorial Diketopyrrolopyrrole−Rylene Supramolecular Films, J. Phys. Chem. C, 2019, 123, 1587−1595

[24] M. B. Smith and J. Michl, Singlet Fission, Chem. Rev., 2010, 110, 6891−6936.

[25] M. C. Hanna and A. J. Nozik, Solar conversion efficiency of photovoltaic and photoelectrolysis cells with carrier multiplication absorbers, J. Appl. Phys., 2006, 100, 074510

[26] D. N. Congreve, J. Lee, N. J. Thompson, E. Hontz, S. R. Yost, P. D. Reusswig, M. E. Bahlke, S. Reineke, T. Van Voorhis and M. A. Baldo, External Quantum Efficiency above 100% in a Singlet-Exciton- Fission−Based Organic Photovoltaic Cell, Science, 2013, 340, 334−337.

[27] P. J. Jadhav, A. Mohanty, J. Sussman, J. Lee and M. A. Baldo, Singlet Exciton Fission in Nanostructured Organic Solar Cells, Nano Lett., 2011, 11, 1495−1498

[28] A. B. Pun, L. M. Campos and D. N. Congreve, Tunable Emission from Triplet Fusion Upconversion in Diketopyrrolopyrroles, J. Am. Chem. Soc., 2019, 141, 3777−3781.

[29] Y. Y. Cheng, B. Fuckel, R. W. MacQueen, T. Khoury, R. G. C. R. Clady, T. F. Schulze, N. J. Ekins-Daukes, M. J. Crossley, B. Stannowski, K. Lips and T. W. Schmidt, Improving the Light- Harvesting of Amorphous Silicon Solar Cells with Photochemical Upconversion, Energy Environ. Sci., 2012, 5, 6953−6959.

[30] J. C. Goldschmidt and S. Fischer, Upconversion for Photovoltaics a Review of Materials, Devices and Concepts for Performance Enhancement, Adv. Opt. Mater., 2015, 3 (4), 510−535

[31] M. A. Green, Third Generation Photovoltaics: Ultra-High Conversion Efficiency at Low Cost, Prog. Photovoltaics Res. Appl., 2001, 9 (2), 123−130

[32] M. Wu, D. N. Congreve, M. W. B. Wilson, J. Jean, N. Geva, M. Welborn, T. Van Voorhis, V. Bulovic, M. G. Bawendi and M. A. Baldo, Solid-State Infrared-to-Visible Upconversion Sensitized by Colloidal Nanocrystals, Nat. Photonics, 2016, 10 (1), 31−34

[33] Y. Il Park, K. T. Lee, Y. D. Suh and T. Hyeon, Upconverting Nanoparticles: A Versatile Platform for Wide-Field Two-Photon Microscopy and Multi-Modal in Vivo Imaging, Chem. Soc. Rev., 2015, 44 (6), 1302−1317

[34] J. D. Bhawalkar, N. D. Kumar, C. F. Zhao and P. N. Prasad, Two- Photon Photodynamic Therapy, J. Clin. Laser Med. Surg., 1997, 15 (5), 201−204

[35] S. L. Oliveira, D. S. Corrêa, L. Misoguti, C. J. L. Constantino, R. F. Aroca, S. C. Zilio and C. R. Mendonça, Perylene Derivatives with Large Two-Photon-Absorption Cross-Sections for Application in Optical Limiting and Upconversion Lasing, Adv. Mater., 2005, 17, 1890−1893

[36] T. N. Singh-Rachford and F. N. Castellano, Photon Upconversion Based on Sensitized Triplet−triplet Annihilation, Coord. Chem. Rev., 2010, 254 (21−22), 2560−2573

[37] R. S. Khnayzer, J. Blumhoff, J. A. Harrington, A. Haefele, F. Deng and F. N. Castellano, Castellano, F. N. Upconversion-Powered Photoelectrochemistry Chem. Commun., 2012, 48 (2), 209−211

[38] R. M. Williams, H. C. Chen, D. Di Nuzzo, S. C. J. Meskers and R. A. J. Janssen, Ultrafast Charge and Triplet State Formation in Diketopyrrolopyrrole Low Band Gap Polymer/Fullerene Blends: Influence of Nanoscale Morphology of Organic PhotovoltaicMaterials on Charge Recombination to the Triplet State, J. Spectrosc., 2017, 1-16

[39] R. Bheerappagari, V. Yeduru, N. Kamatham, V. Munisamy, H. Mandal, S. P. Singh and P. R. Bangal, Ultrafast Fluorescence Photoswitch Incorporating Diketopyrrolopyrrole and Benzo[1,3]oxazine, J. Phys. Chem. C, 2017, 121, 27313−27326

[40] S. M. Aly, S. Goswami, Q. A. Alsulami, K. S. Schanze and O. F. Mohammed, Ultrafast Photoinduced Electron Transfer in a π-Conjugated Oligomer/Porphyrin Complex J. Phys. Chem. Lett., 2014, 5, 3386−3390

[41] A. Q. Alsulami, M. S. Aly, S. Goswami, E. Alarousu, A.Usman, S. K. Schanze and F. O. Mohammed, Ultrafast excited-state dynamics of diketopyrrolopyrrole (DPP)-based materials: static versus diffusion controlled electron transfer process, J. Phys. Chem. C , 2015, 119, 15919−15925

[42] Y. Venkatesh, M. Venkatesan, B. Ramakrishna and P. R. Bangal, Ultrafast Time-Resolved Emission and Absorption Spectra of meso-Pyridyl Porphyrins upon Soret Band Excitation Studied by Fluorescence Up-Conversion and Transient Absorption Spectroscopy, J. Phys. Chem. B, 2016, 120, 9410−9421

[43] I. H. Van Stokkum, B. Van Oort, F. Van Mourik, B. Gobets and H. Van Amerongen, Biophysical Techniques in Photosynthesis,Springer, 2008, p. 223.

[44] I. H. Van Stokkum, D. S. Larsen and R. van Grondelle,Global and target analysis of time-resolved spectra Biochim. Biophys. Acta, Bioenerg., 2004, 1657, 82-104

[45] S. P. Laptenok, J. W. Borst, K. M. Mullen, I. H. van Stokkum, A. J. Visser and H. van Amerongen, Global analysis of Förster resonance energy transfer in live cells measured by fluorescence lifetime imaging microscopy exploiting the rise time of acceptor fluorescence. Phys. Chem.Chem. Phys., 2010, 12, 7593-7602.

[46] K. M. Mullen and I. H. Van Stokkum,An Introduction to the Special Volume "Spectroscopy and Chemometrics in R" J. Stat. Soft., 2007,18, 1

[47] J. Snellenburg, S. Laptenok, R. Seger, K. Mullen and I. Van Stokkum,Glotaran: A Java-Based Graphical User Interface for the R Package TIMPJ. Stat. Soft., 2012, 49, 3.

[48] D. Bharath, S. Chithiravel, M. Sasikumar, N. R. Chereddy, B. Shanigaram, K. Bhanuprakash, K. Krishnamoorthy and V. J. Rao, A detailed study on the thermal, photo-physical and electrochemical properties and OFET applications of D–π–A–π–D structured unsymmetrical diketopyrrolopyrrole materials, RSC Adv., 2015, 5, 94859–94865

[49] J. Dhar, N. Venkatramaiah, A. Anitha and S. Patil, Photophysical, electrochemical and solid state properties of diketopyrrolopyrrole based molecular materials: importance of the donor group, J. Mater. Chem. C, 2014, 2, 3457

[50] F. Pop, W. Lewis and D. B. Amabilino, Solid state supramolecular structure of diketopyrrolopyrrole chromophores: correlating stacking geometry with visible light absorption, CrystEngComm, 2016, 18, 8933-8943

[51] C. Ji, L. Yin, K. Li, L. Wang, X. Jiang, Y. Sun and Y. Li, D−π− A−π−D-type low band gap diketopyrrolopyrrole based small molecules containing an ethynyl-linkage RSC Adv., 2015, 5, 31606−31614

[52] S. Y. Liu, M. M. Shi, J. C. Huang, Z. N. Jin, X. L. Hu, J. Y. Pan, H. Y. Li, A. K. Y. Jen and H. Z. Chen, C−H activation: making diketopyrrolopyrrole derivatives easily accessible, J. Mater. Chem. A, 2013, 1, 2795−2805.

[53] Goswami, S.; Winkel, R. W.; Alarousu, E.; Ghiviriga, I.;Mohammed, O. F.; Schanze, K. S. Photophysics of Organometallic Platinum(II) Derivatives of the Diketopyrrolopyrrole Chromophore, J. Phys. Chem. A 2014, 118, 11735-11743

[54] McCusker, C. E.; Hablot, D.; Ziessel, R.; Castellano, F. N. Triplet State Formation in Homo- and Heterometallic Diketopyrrolopyrrole Chromophores, Inorg.Chem. 2014, 53, 12564-12571

[55] D. Rehm, A. Weller, Kinetics of Fluorescence Quenching by Electron and H-atom Transfer, Isr. J. Chem., 1970, 8, 259−271

[56] Y. Che, W. Ma, H. Ji, J. Zhao and L. Zang, Visible Photooxidation of Dibenzothiophenes Sensitized by 2-(4-Methoxyphenyl)-4, 6-diphenylpyrylium: An Electron Transfer Mechanism without Involvement of Superoxide, J. Phys. Chem. B, 2006, 110, 2942-2948

[57] M. A. Naik, N. Venkatramaiah, C. Kanimozhi, S Patil, Influence of Side-Chain on Structural Order and Photophysical Properties in Thiophene Based Diketopyrrolopyrroles: A Systematic Study, J. Phys.Chem. C, 2012, 116, 26128-26137

[58] C. E. Miller, M. R. Wasielewski and G. C. Schatz, Modeling Singlet Fission in Rylene and Diketopyrrolopyrrole Derivatives: The Role of the Charge Transfer State in Superexchange and Excimer Formation, J. Phys. Chem. C, 2017, 121, 10345−10350

[59] Md. M. Alam, F. Bolze, C. Daniel, L. Flamigni, C. Gourlaouen, V. Heitz,S. Jenni, J. Schmitt, A. Sourd and B. Ventura, π-Extended diketopyrrolopyrrole–porphyrin arrays: one- and two-photon photophysical investigations and theoretical studies Phys. Chem. Chem. Phys., 2016, 18, 21954—21965

[60] T. Roland, E. Heyer, L. Liu, A. Ruff, S. Ludwigs, R. Ziessel and S. Haacke, A Detailed Analysis of Multiple Photoreactions in a Light-Harvesting Molecular Triad with Overlapping Spectra by Utrafast Spectroscopy J. Phys. Chem. C ,2014, 118, 24290−24301

[61] M. R. Son, J-Y. Cho, Y-S. Kim, J-H. Son, D. W. Cho and S. O. Kang, Direct observation of the photoinduced electron transfer processes of bis(4-arylphenylamino benzo)-ortho-

carborane using transient absorption spectroscopic measurements, Phys. Chem. Chem. Phys., 2017, 19, 24485-24492

[62] A. Ruff, E. Heyer, T. Roland, S. Haacke, R. Ziessel and S. Ludwigs, Electrochemical and optical properties of molecular triads based on triphenylamine, diketopyrrolopyrrole and boron-dipyrromethene Electrochimica Acta, 2015, 173, 847–859.